Environ Geochem Health (2022) 44:3297–3320
https://doi.org/10.1007/s10653-021-01083-x

ORIGINAL PAPER

May a comprehensive mineralogical study of a jackstone calculus and some other human bladder stones unveil health and environmental implications?

M. Mercurio · F. Izzo · Giacomo Diego Gatta · L. Salzano · G. Lotrecchiano · P. Saldutto · C. Germinario · C. Grifa · E. Varricchio · A. Carafa · Maria Chiara Di Meo · A. Langella

Received: 18 May 2021 / Accepted: 24 August 2021 / Published online: 16 September 2021

Abstract This paper represents the first result of an active collaboration between the University of Sannio and the *San Pio* Hospital (Benevento, Italy), started in the 2018, that aims to a detailed mineralogical investigation of urinary stones of patients from Campania region. Herein, selected human bladder stones have been deeply characterized for clinical purposes and environmental biomonitoring, focusing on the importance to evaluate the concentration and distribution of undesired trace elements by means of microscopic techniques in the place of conventional wet chemical analyses. A rare bladder stone with a sea-urchin appearance, known as jackstone calculus, were also investigated (along with bladder stones made of uric acid and brushite) by means a comprehensive analytical approach, including Synchrotron X-ray Diffraction and Simultaneous Thermal Analyses. Main clinical assumptions were inferred according to the morpho-constitutional classification of bladder stones and information about patient's medical history and lifestyle. In most of the analyzed uroliths, undesired trace elements such as copper, cadmium, lead, chromium, mercury and arsenic have been detected and generally attributable to environmental pollution or contaminated food. Simultaneous occurrence of selenium and mercury should denote a methylmercury detoxification process, probably leading to the formation of a very rare HgSe compound known as tiemannite.

Keywords Bladder stones · Jackstone calculus · Sea-urchin appearance · EMPA-WDS · Synchrotron radiation · HgSe

Supplementary Information The online version contains supplementary material available at https://doi.org/10.1007/s10653-021-01083-x.

M. Mercurio · F. Izzo (✉) · C. Germinario · C. Grifa · E. Varricchio · A. Carafa · M. C. Di Meo
Dipartimento di Scienze E Tecnologie, Università degli Studi del Sannio, Via F. De Sanctis, 82100 Benevento, Italy
e-mail: francesco.izzo@unisannio.it

G. D. Gatta
Dipartimento Scienze della Terra, Università degli Studi di Milano, Via Botticelli 23, 20133 Milan, Italy

L. Salzano · G. Lotrecchiano · P. Saldutto
UOC Urologia, Azienda Ospedaliera San Pio di Benevento, Via dell'Angelo 82100, Benevento, Italy

A. Langella
Dipartimento di Scienze della Terra, dell'Ambiente e delle Risorse, Università degli Studi di Napoli Federico II, Complesso Universitario Di Monte Sant'Angelo, Edificio 10, Via Vicinale Cupa Cintia 21, 80126 Naples, Italy

Introduction

Urolithiasis distresses Western population with an incidence of up to about 20%. The phenomenon has been addressed in medicine since the early 1800s,

although evidence of a bladder stone dates back to the prehistoric period (Moran, 2014). Nowadays, several studies have been published (Chatterjee et al., 2018; Daudon et al., 2016; Kumar et al., 2006; Primiano et al., 2014) and mostly conducted in order to contribute to the improvement of the clinical treatment of this painful pathology with impacting social and economic implications (Ansari & Gupta, 2003; Giannossi et al., 2012). From an epidemiological point of view, in addition to the geographical location, other key factors to consider are: gender, race, age, familiarity, diet (included drinking water quality), smoking, climate, occupation and physical activity (Afaj & Sultan, 2005; Curhan et al., 1998; Hornberger & Bollner, 2018; Keshavarzi et al., 2016; Liu et al., 2020). It is almost certain that most of the people suffering from this disease are white, males, between 40 and 50 years old, observing diets rich in animal proteins, sedentary and living in warm and humid regions (Abboud, 2008; Keshavarzi et al., 2016). Within this frame, Italian population seems to be particularly predisposed to such forms of urolithiasis (up to 9% of the population reports cases), as evidenced by an estimated incidence of 100 k new cases per year stimulating the scientific community to always proceed to investigations taking into account the aforementioned key factors (Giannossi, 2013).

Main actors of urolithiasis are polyphasic biominerals mixed with organic phases consisting, as reported by Daudon et al. (Daudon et al., 2016), of calcium oxalates, calcium phosphates, urates and uric acid, and other rare phases (e.g., cystine, proteins, purines or rare drugs).

Formation of urinary stones is determined by a combination of different processes, from supersaturation followed by nucleation, the latter enhanced by the activity of inhibitors (e.g., magnesium, citrate ions) and promoters (e.g., calcium, organic compounds such as cholesterol) (Basavaraj et al., 2007; Singh & Rai, 2014). Hence, the need to address the issue with a multidisciplinary approach: a new geobiological model on the dissolution of kidney stones in vivo has recently been proposed, shedding new light on clinical implications (Sivaguru et al., 2018). "Give me your stone, I will tell you who you are" was the title of an interesting study by Cloutier et al., (2015), which highlighted the importance of a thorough analytical characterization at the basis of a correct etiology, unveiling the minerogenetic processes underlying kidney stones. This interesting approach highlights two important aspects: (1) which information from stone analysis could be clinically relevant and (2) the keys for interpretation of stone analysis. In other words, the urinary stone can be likely defined as an environmental geo-bio-marker and its in-depth analytical characterization may provide useful information regarding the anamnesis of the patient. To achieve this goal, the scientific community requires the application of an approach typical of mineralogical sciences, as suggested for the first time by Prien and Frondel (1947). Several analytical techniques have been used to collect chemical, mineralogical and textural data for urinary stones: Scanning Electron Microscopy coupled with Energy Dispersive Spectroscopy or Wavelength Dispersive Spectroscopy analysis (SEM/EDS or WDS), X-ray Diffraction (XRD), Infrared spectroscopy (IR), thermal analyses, computed tomography, polarized light and stereoscopic microscopy, and image analysis (Ancharov et al., 2007; Li et al., 2013; Mukherjee, 2014; Nair & Ninan, 1978; Shiekh et al., 2006). Nevertheless, a limit to this approach is due to (i) a usually low amount (few milligrams) of sample and (ii) the lack of comprehensive and comparative studies reporting data from all the techniques above described. Actually, it is necessary to remark that a reliable laboratory analysis should provide, beyond a mineralogical classification, also a chemical characterization concerning the content of alkaline, earth-alkaline and heavy metals (e.g., Hg, As, Pb, Cd, etc.). In fact, it has been shown that trace elements can be markers of environmental risks also representative of the trigger factors involved in urinary stones formation (Abboud, 2008; Giannossi et al., 2013; Keshavarzi et al., 2015; Kuta et al., 2013; Öhman et al., 1992).

Based on this premises and considering the very few studies giving information on bladder stones, especially indicative of Italian patients (Giannossi, 2013), the present research offers a multi-methodological approach aimed at a deeply mineralogical characterization of selected human bladder stones, available thanks to an active collaboration with the Department of Urology of *San Pio* Hospital in Benevento, Italy. The primary purpose of this investigation was to verify the existence of correlations between the studied biominerals and the association of major (> 1 wt.%) and trace (< 1 wt.%) elements, including "exotic" metals that can be crucial for the

assessment of a potential environmental/food contamination.

The bladder stones

Most urinary stones are located in the kidney but a small fraction (ca. 5%) grows inside the ureter and bladder. Those who suffer most are males from developed countries with a bimodal trend: children and adults over 60 years of age. According to EUA guidelines (Türk et al., 2019), bladder stones can be classified as primary, secondary or migratory, as a consequence of a multifactorial etiology. Primary bladder stones (also known as endemic bladder stones) are typically observed in children, in absence of urinary tract pathologies. Secondary bladder stones can be due to several causes, such as bladder outlet obstruction due to benign prostatic enlargement (BPE), urethral stricture or other urinary tract abnormalities. In some cases, urinary stones that formed in the upper urinary tract can reach the bladder becoming a *nidus* for bladder stones.

Bladder stones represent a non-negligible set of biominerals, having quite amazing features. Referring to the classification of urinary stones by Daudon et al. (2016), there are seven morpho-constitutional types: type I (a, b, c, d, e) Calcium Oxalate Monohydrate (COM), type II (a, b, c) Calcium Oxalate Dihydrate (COD), type III (a, b, c, d) uric acid and urate, type IV (a1, a2, b, c, d) phosphate, type V (a, b) cystine, type VI (a, b, c) protein and Type VII miscellaneous stones.

Jackstone calculus, commonly reported in veterinary and rarely in human literature (Perlmutter et al., 2002; Singh et al., 2011), is a rare bladder subtype of urinary stone with a sea-urchin appearance or resembling a toy jacks. It is almost always composed of calcium oxalate dehydrate, characterized by a dense central core and radiating spicules (Sweeney & Dyer, 2015). As far as investigation of Italian bladder stones are concerned, rare case studies have been reported so far (Brogna et al., 2019), thus leaving some questions related to mineralogical aspects still debated.

Materials and methods

Biominerals

Bladder stone samples have been surgically collected from six male patients admitted to the Department of Urology of the *San Pio* Hospital (Benevento, Italy) in 2020. Clinical interviews were also held, in anonymous form, in order to gather some useful information about patient's medical history and lifestyle (Table 1). All the patients (67–76 years old are resident in Campania region) were affected by moderate-severe lower urinary tract symptoms (LUTS) whereas the patient KS012B reported hematuria. Only one patient states to have a desk job (employed), whereas the remaining ones are farmers, barman or retired. None of the patients has a regular physical activity. Considering their body weight and height, the BMI (Body Mass Index) ranges from 25.3 (KS011B) to 29.4 kg/m^2 (KS012B) that, according to the World Health Organization, define them as overweight. Furthermore, they suffer from a large variety of diseases such as diabetes (KS011B), arteriosclerotic heart disease (KS012B), dyslipidemia (KS020B) and hypertension (KS006B and KS023B). As far as eating habits are concerned, all patients state to get carbohydrates and protein foods (meat, eggs and cheese) at least once per week or more, and less frequently vegetables. They also drink wine and coffee every day, and moderately beer and other alcohols. Only one patient drinks exclusively tap water (KS022B).

Bladder stones were selected as a function of the availability of material (weight ranging from 0.5 to 9.7 g) in order to ensure a complete chemical, mineralogical and petrographic characterization (Table 2). Before the analyses, bladder stones have been washed thoroughly with distilled water, sterilized in pure ethanol and then dried at room temperature.

Laboratory strategy

Preliminary morphological description of bulk bladder stones has been carried out by means of a NIKON SMZ 1000 stereomicroscope connected to a NIKON digital Sight DSRi2 camera. Polarized Light Microscopy (PLM) observations carried out on thin sections (ca. 30 μm) using a Nikon Eclipse 6400 POL microscope equipped with a Nikon DS-Fi camera provided information on the microtextural features and the mineralogical composition of the bladder stones. Chemical phases were detected on powdered samples (a few milligrams) by Fourier Transform Infrared Spectroscopy (FTIR) performed in Attenuated Total Reflectance mode (ATR) by means of a Bruker ALPHA-R spectrometer (Bruker Opus 7.2 software)

Table 1 Patient's personal details

n	ID	Gender	Age	Occupation	Physical activity	Body weight	Height	BMI*	Weight of the calculus
1	KS006B	Male	76	Retired	No	78 kg	175 cm	25.5 kg/m^2	1.09 g
2	KS011B	Male	75	Farmer	No	69 kg	165 cm	25.3 kg/m^2	0.53 g
3	KS012B	Male	73	Farmer	No	90 kg	175 cm	29.4 kg/m^2	1.55 g
4	KS020B	Male	67	Barman	No	78 kg	165 cm	28.6 kg/m^2	1.05 g
5	KS022B	Male	76	Farmer	No	74 kg	170 cm	25.6 kg/m^2	3.15 g
6	KS023B	Male	75	Employed	No	75 kg	165 cm	27.6 kg/m^2	9.75 g

*Body Mass Index

Table 2 List of analytical techniques used for the morpho-constitutional classification of bladder stones

Analytical technique	Abbreviation	Detectable features	Targets
Stereomicroscopy	SM	Morphological examination of surface and inner organization of calculus	Texture
Polarized light microscopy	PLM	Shape, size and optical properties of species	Mineralogical composition, texture
Electron-microprobe analyses coupled to wavelength dispersive spectroscopy	EMPA/WDS	Occurrence and relative concentration of major and trace elements	Elemental chemical composition, texture
Synchrotron X-ray diffraction	XRD	Crystal lattice parameters	Mineralogical composition
Fourier Transform Infrared spectroscopy	FTIR	Molecular vibrations of functional groups	Molecular chemical composition
Simultaneous Thermal Analyses	STA	Mass changes, thermal stability, reaction kinetics, endo-exothermic reactions, composition of evolved gases	Chemical–mineralogical composition

in the mid-infrared spectral range (4000–400 cm^{-1}, 64 scans, 4 cm^{-1} resolution).

For a crystalline phase identification of the aforementioned samples, X-ray powder diffraction data were collected at the XPRESS beamline of the ELETTRA Synchrotron radiation facility (Trieste, Italy) (Lotti et al., 2020). Data collections were performed by a monochromatic and polarized circular beam, with a wavelength of 0.4957 Å and a diameter of ca. 50 µm. Powder samples were loaded in B-glass capillaries (300 µm in diameters). A MAR345 image plate detector was used, positioned at 340 mm from the sample. The following collection strategy was adopted: the capillary was rotated from − 5 to + 5° around the (vertical) ω -axis for an exposure time of 60 s. The 2D powder diffraction rings, collected in transmitting geometry, were converted into 2-theta *vs.* intensity plots, using the Fit2D software (Hammersley, 2016). Geometrical parameters were previously refined based on the XRD pattern of the LaB_6 calibrant. The preliminary identification of the crystalline components was performed using the suite of programs X'Pert-HighScore (Panalytical).

Major and trace elements were quantitatively detected via electron-microprobe analyses obtained from polished and carbon-coated thin sections (ca. 30 µm) using a JEOL JXA-8200 microprobe in wavelength dispersive mode (EMPA/WDS). The system was operated using an accelerating voltage of 15 kV, a counting time of 30 s on the peaks and 10 s on the backgrounds. EMPA-WDS quantifications were carried out using the following standards: omphacite for Na, celestine for Sr, rhodonite Mn, orthoclase for K, forsterite-154 for Mg, nickeline for

As and Ni, mercury selenide for Hg and Se, fayalite-143 for Fe, grossular for Ca and Al, galena for Pb, apatite for P, and pure elements for Cd, Sb, Cu, Cr and Zn.

The thermal behavior of bladder stones (from 30 to 60 mg of powdered sample) was investigated by Simultaneous Thermal Analyses (STA) TG-DSC (NETZSCH STA 449 F3 Jupiter) coupled with a FTIR BRUKER Tensor 27 for the Evolved Gas Analysis (EGA) by a transfer line heated at 200 °C. The samples were heated from 40 to 1050 °C, with a heating rate of 10 °C/min in pure air atmosphere (flow rate 60 mL/min). Data have been processed with NETZSCH Proteus 6.1and Bruker Opus 7.0 software. FTIR analyses of thermal products at different decomposition temperatures were also carried out and discussed in the text, as well as in supplementary materials.

Results

Optical microscopy

Stereomicroscopy

The observation of urinary stones by means of a stereomicroscope represents a first fundamental approach in their characterization, providing important information in terms of etiological or pathophysiological conditions (Daudon et al., 2016). This examination is based on a morphological evaluation of the aggregates, taking into account color, shape, aspect of the surface and the section, presence of umbilication (papillary imprint) and Randall's Plaque (Abrol & Kekre, 2014; Çiftçioğlu et al., 2008; Letavernier et al., 2016).

Figure 1 reports selected micrographs of the examined bladder stones. KS006B shows a light-colored rough surface with radial crystallization and not well-defined concentric layers in the inner part (Fig. 1a and b). Sample KS011B shows an orange, compact and concentric microstructure with a radiating organization, interested by sporadic brownish intercalations. This sample exhibits a homogeneous smooth surface (Fig. 1c). KS012B displays a sea-urchin appearance and a particular brown spiculated surface (Fig. 1d), with a finely granular and poorly organized section (Fig. 1e). In KS020B, the brown-orange concentric structure is poorly organized with thin porous and orange layers (Fig. 1f, g and h). A heterogeneous coloration, from beige to brown-orange, is observed for the rough surface of KS022B, which clearly shows an orange concentric structure with radial organization (Fig. 1i and j). Lastly, the fragments forming KS023B exhibit a compact concentric internal structure with a radiating organization, along with frequent small orange-brown inclusions (Fig. 1k). The color is not homogeneous, ranging from pale yellow to whitish. A quite smooth surface can be also observed (Fig. 1l).

Polarized light microscopy

Further information about the internal microstructure and mineralogical nature for the examined bladder stones can be inferred by means of Polarized Light Microscopy (PLM). In order to describe shape, size and optical properties (birefringence, cleavage, extinction, etc.) of mineralogical species, bladder stones were thin-sectioned parallel to the concentric layers, in order to investigate even the central portion of the samples, where the *nuclei* usually occur.

The sea-urchin appearance of KS012B is still recognizable in thin section (Fig. 2a). The internal concentric pattern of this sample appears well-defined but irregular and poorly organized, suggesting the occurrence of different nucleation centers. It is composed by subhedral or anhedral crystals with high interference colors (Fig. 2b), consistent with the optical properties of calcium oxalate (i.e., whewellite) aggregates (Giannossi, 2013; "mindat.org" n.d.-a).

KS006B displays a weakly consistent internal structure made of acicular crystal of brushite (Fig. 2c and d). This mineral species shows a low surface relief, a perfect cleavage and first order interference colors ("mindat.org" n.d.-b). Furthermore, this aggregate is interested by the presence of darker layers, likely made of amorphous/organic substances.

The remaining samples (KS011B, KS020B, KS022B and KS023B) are generally similar each other as they exhibit a more or less compact concentric structure, with colors ranging from dark brown to pale yellow (Fig. 2e and f). In crossed polars, the aggregates display not well-defined interference colors, ranging from grayish to yellowish. These features are usually consistent with uric acid aggregates (Giannossi, 2013; Ringertz, 1965).

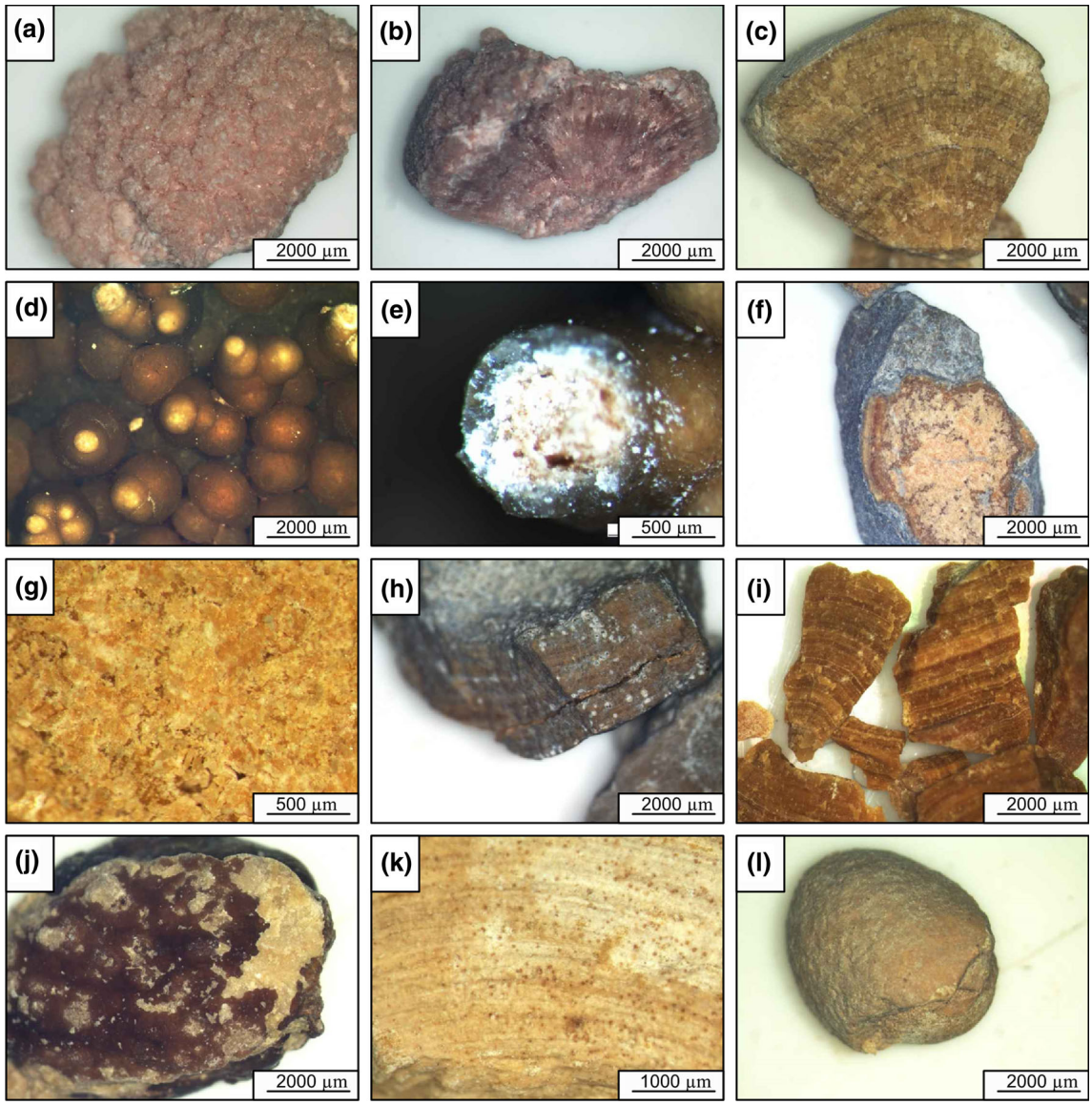

Fig. 1 Micrographs of bladder stones captured in stereomicroscopy: **a** and **b** KS006B; **c** KS011B; **d** and **e** KS012B; **f**, **g** and **h** KS020; **i** and **j** KS022B; **k** and **l** KS023B

Fourier transform infrared spectroscopy

FTIR measurements on bulk powdered samples provide a first reliable characterization, at the atomic scale, of urinary stones (Gràcia-Garcia et al., 2011; Muschietti et al., 2016; Schnitzler et al., 2004; Schubert, 2006; Wilson et al., 2010). Absorption bands of the bladder stones examined in the present investigation are summarized in Table 3, whereas in Fig. 3 their FTIR spectra (ATR mode) are shown. Excluding some shared signals, the results clearly highlighted the compositional differences between the analyzed biominerals.

Samples KS011B, KS020B, KS022B and KS023B display the same pattern, fully compatible with that of uric acid $C_5H_4N_4O_3$ (Primiano et al., 2014). Particularly interesting are the absorption bands assigned to the N–H stretching vibrations (Aslin Shamema et al., 2015; Sekkoum et al., 2016), such as those at ca. 3086 cm^{-1}, 2994 cm^{-1}, 2915 cm^{-1}, 2788 cm^{-1},

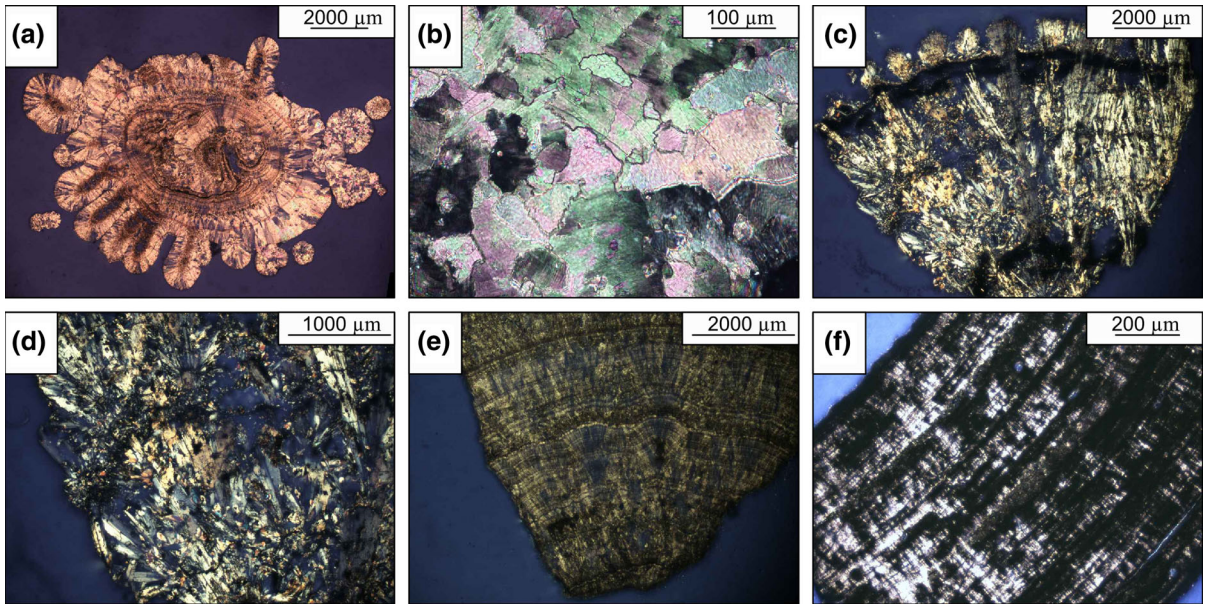

Fig. 2 Micrographs of bladder stones captured in polarized light microscopy: **a** internal structure and **b** detail of calcium oxalate crystals for sample KS012B; **c** and **d** brushite crystals in sample KS006B; **e** and **f** uric acids KS011B and KS023B

2685 cm^{-1} and 2604 cm^{-1} standing on a broad band between 3300–2800 cm^{-1}. The remaining absorption bands describe a very dense sequence of narrowed signals in the fingerprint region, approximately between 1800–400 cm^{-1} (Fig. 3).

Different spectroscopic features were observed for the samples KS006B and KS012B. The former shows the typical FTIR spectrum of the mineral brushite $CaHPO_4{\cdot}2(H_2O)$ (Hirsch et al., 2014; Mandel & Tas, 2010; Suryawanshi & Chaudhari, 2014). As a whole, the absorption bands at higher wavenumbers indicate the stretching (3542 cm^{-1} and 3474 cm^{-1}) and bending (1664 cm^{-1}) vibrations of H_2O molecules. On the other hand, absorption bands in the fingerprint region are mainly due to the HPO_4 group. The peak at 1205 cm^{-1} is assigned to H in plane bending vibration, whereas the signals at 1135 cm^{-1}, 1059 cm^{-1}, 986 cm^{-1} and 872 cm^{-1} are due to P–O stretching vibrations. The bands at 577 cm^{-1} and 523 cm^{-1} could be ascribed to the O–P–O bending vibrations. In spite of the high correlation of the FTIR spectrum of the sample KS006B with those reported in literature (Hirsch et al., 2014; Mandel & Tas, 2010; Suryawanshi & Chaudhari, 2014), some bands in the fingerprint region did not perfectly fit the typical expected wavenumbers. This mismatch is likely due to some ionic substitutions or to the occurrence, in this sample, of other chemical compounds (i.e., CaOx and CaP phases). Moreover, the additional occurrence of a band at 1323 cm^{-1} (Table 3) is probably due to the presence of CaOx inclusions.

As far as sample KS012B is concerned, FTIR measurements suggest the typical composition of a calcium oxalate (Conti et al., 2010; Sekkoum et al., 2016; Selvaraju et al., 2015). The main diagnostic bands of this species lie at ca. 1610 cm^{-1} (C=O vibration), 1313 cm^{-1} (C-O vibration), 886 cm^{-1} (C–C stretching), 779 cm^{-1} (C–H bending), 656 cm^{-1} (O–H bending), 511 cm^{-1} (in-plane O–-C=O bending). Spectra also showed a sequence of absorption bands at higher wavenumbers (3440 cm^{-1}, 3318 cm^{-1}, 3225 cm^{-1} and 3043 cm^{-1}), ascribable to symmetric and asymmetric O–H stretching vibrations. According to the previous experimental findings (Kanchana et al., 2009), the high intensities of the absorption bands at 779 cm^{-1} and 511 cm^{-1} allow to infer the occurrence, in sample KS012B, of the mineral whewellite (calcium oxalate monohydrate $CaC_2O_4{\cdot}H_2O$). Lastly, a very weak absorption band at ca. 1044 cm^{-1} can be also observed mainly attributable to occurrence of calcium phosphate (Table 3).

Table 3 FTIR data of bladder stones (expressed in cm^{-1}). Note: br = broad; vs = very strong; s = strong; sh = shoulder; m = medium; w = weak

KS006B	KS011B	KS012B	KS020B	KS022B	KS023B	Chemical phases
3542 w						Brushite
3474 w						Brushite
		3440 w				Calcium oxalate
3268 w						Brushite
		3318 w				Calcium oxalate
		3225 w				Calcium oxalate
3155 w						Brushite
	3089 sh		3084 sh	3082 sh	3088 sh	Uric Acid
		3043 w				Calcium oxalate
	2983 m		2996 m	2992 m	3005 m	Uric Acid
	2918 w		2912 w	2914 w	2917 w	Uric Acid
	2788 m		2785 m	2787 m	2793 m	Uric Acid
	2687 m		2680 m	2687 m	2684 m	Uric Acid
	2605 sh		2609 sh	2600 sh	2603 sh	Uric Acid
	1661 vs		1654 vs	1662 vs	1662 vs	Uric Acid
1644 w						Brushite
		1610 vs				Calcium oxalate
	1584 s		1585 s	1584 s	1585 s	Uric Acid
	1435 m		1434 m	1435 m	1435 m	Uric Acid
	1398 m		1399 m	1399 m	1399 m	Uric Acid
		1380 vw				Calcium oxalate
	1347 m		1347 m	1347 m	1347 m	Uric Acid
1323 vw						Calcium oxalate
		1313 vs				Calcium oxalate
	1301 m		1302 m	1301 m	1302 m	Uric Acid
1205 m						Brushite
1135 m						Brushite
	1121 m		1121 m	1121 m	1121 m	Uric Acid
1059 s						Brushite
		1044 vw				Calcium phosphate
	1025 w		1026 w	1025 w	1026 w	Uric Acid
	990 m		990 m	990 m	990 m	Uric Acid
986 m						Brushite
		952 vw				Calcium oxalate
		886 w				Calcium oxalate
872 w	875 w		876 w	875 w	875 w	Uric Acid/Brushite
784 w	779 m	779 vs	781 m	779 m	780 m	Uric Acid/Calcium oxalate/Brushite
	742 s		743 s	742 s	743 s	Uric Acid
	703 s		702 s	703 s	703 s	Uric Acid
655 vw		656 m				Calcium oxalate/Brushite
	617 m		617 m	617 m	617 m	Uric Acid
		597 m				Calcium oxalate
577 w	572 m		572 m	571 m	572 m	Uric Acid/Brushite
523 vs	519 m		519 m	520 m	520 m	Uric Acid/Brushite
		511 s				Calcium oxalate
	470 vs		471 vs	469 vs	470 vs	Uric Acid

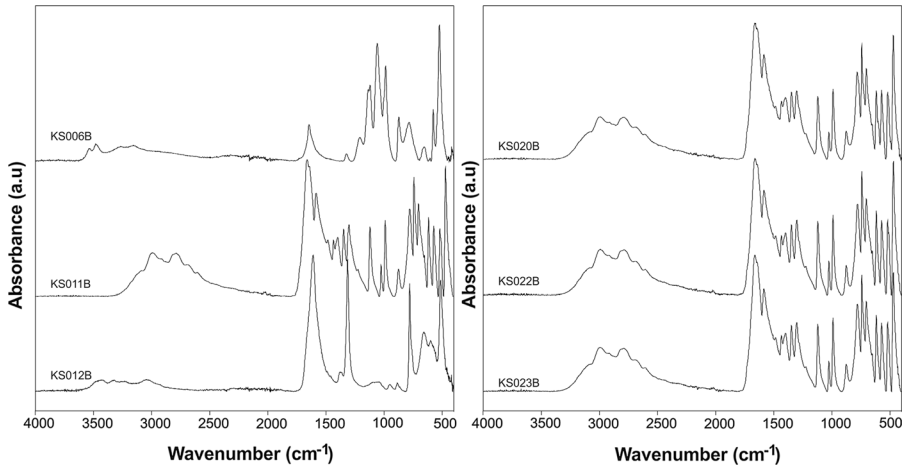

Fig. 3 FTIR spectra of analyzed bladders: KS006B (brushite), KS011B (uric acid), KS012B (calcium oxalate) KS020 (uric acid), KS022B (uric acid) and KS023B (uric acid)

Synchrotron X-ray Diffraction (XRD)

The X-ray diffraction patterns (2-theta range: 3–40°, λ = 0.4957 Å) were successfully indexed (Figs. 4 and 5) and ascribed as follow: KS006B is substantially composed by brushite [$Ca(HPO_4)\cdot 2H_2O$, $a \cong 6.36$, $b \cong 15.19$, $c \cong 5.81$ Å, $\beta \cong 118.4°$, sp. gr. *C*2/*c*] and weddellite [$CaC_2O_4\cdot(2.5\text{-}x)H_2O$, $a \cong 12.37$, $c \cong 7.36$ Å, sp. gr. *I*4/*m*], and minor evidence ascribable to the presence of whewellite [$CaC_2O_4\cdot H_2O$, $a \cong 6.29$, $b \cong 14.58$, $c \cong 10.12$, $\beta \cong 109.46$, sp. gr. $P2_1/c$]. In particular, the most intensive peak of whewellite (at 2-theta ≅ 4.753°) lies on the shoulder of the most intensive peak of weddellite (at 2-theta ≅ 4.576°) (Fig. 5). Samples KS011B, KS020B, KS022B and KS023B are substantially composed by uric acid [$C_5H_4N_4O_3$, $a \cong 14.46$, $b \cong 7.40$, $c \cong 6.21$ Å, $\beta \cong 65.10°$, sp. gr. $P2_1/a$]. Except for KS011B, very minor evidence, potentially ascribable to the presence of whewellite, can be also considered. Lastly, KS012B seems to be mainly composed by whewellite. The full-width-at-half-maximum (FWHM, estimated by Le Bail full-profile fit; (Le Bail et al., 1988) of the brushite peaks is about 0.22°, whereas the diffraction peaks of uric acid (FWHM ≅ 0.14°) and weddellite (FWHM ≅ 0.15°) are significantly sharper.

EMPA/WDS

Chemical data here provided (Table 4) reflect the occurrence and relative concentration of both major and some peculiar trace elements, as well as their distribution in the bladder stones.

Although mainly formed by brushite, as detected by FTIR and XRD analyses, chemical and mineralogical composition of sample KS006B appears quite heterogeneous in EMPA/WDS (Figs. 6 and 7), showing the occurrence of acicular and radiating crystals of brushite (Ca ∼ 23.5 wt.%, P ∼ 18.0 wt.%), along with bipyramidal crystals of calcium oxalate (Ca ∼ 30.9 wt.%) (Table 4). This bladder stone also displays the occurrence of spheroidal particles (< 10 µm) composed by calcium (∼ 32.25 wt.%) and phosphorous (∼ 17.5 wt.%), characterized by an internal concentric structure and mainly located into the cavities (Fig. 6).

Ca-phosphate inclusions (Ca, 33.83 wt.%; P, 15.70 wt.%) can be also observed for the sea-urchin calculus (KS012B), at the interface between its internal multi-nucleus structure and the external budding surface (Fig. 6). The remaining part of this bladder stone is composed by calcium oxalate (Ca ∼ 30.23 wt.%) (Table 4).

Inclusions of Ca-oxalate and Ca-phosphate in uric acid bladder stones (KS011B, KS020B, KS022B and KS023B) are scattered along the layers forming the internal concentric structure (Fig. 6). In sample KS011B, a compact layer of calcium oxalate is clearly observed between uric acid levels (Fig. 6).

As far as trace elements are concerned, the occurrence of alkali metals such as Na and K can be observed in all the mineral species forming the

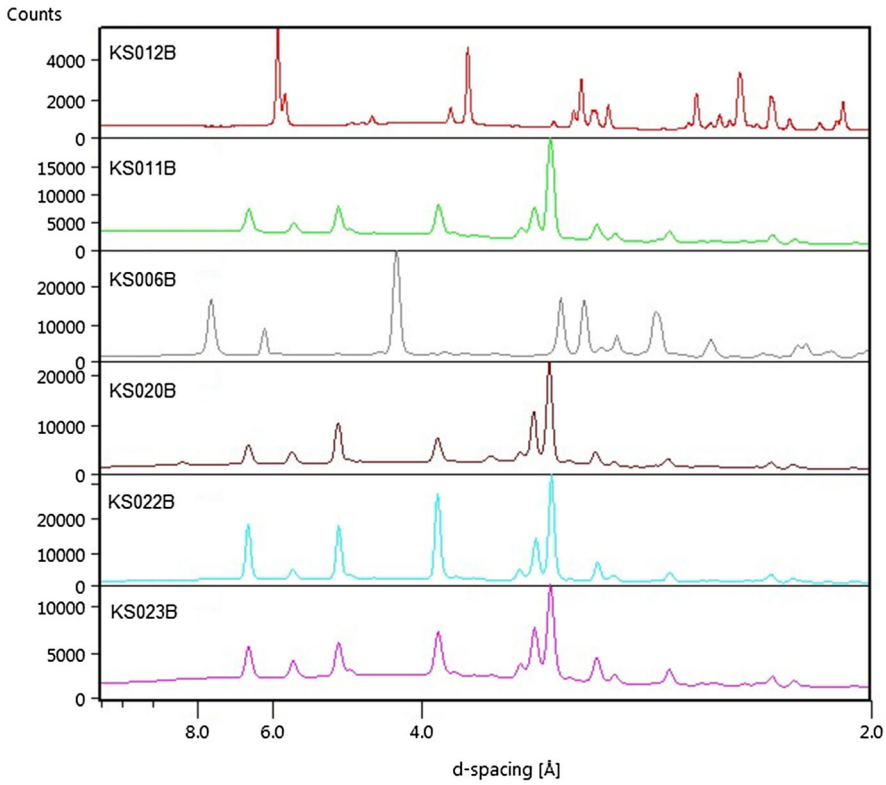

Fig. 4 Synchrotron X-ray powder diffraction patterns [d-spacing (Å) vs. intensity (counts)] pertaining to the samples KS006B, KS011B, KS012B, KS020B, KS022B and KS023B (λ = 0.4957 Å)

examined samples (Fig. 7 and Table 4). Nevertheless, their concentration in Ca-phosphate inclusions was generally higher than those measured in oxalates and uric acids. The same goes for the alkali-earth metal Mg and transition metal Zn, whereas Sr is generally more abundant in calcium oxalates. Iron, and less frequently Mn, is mainly concentrated in Ca-P and Ca-Ox phases. Aluminum and antimony were also detected in most of analyzed points, whereas nickel was only found in sample KS012B (CaOx urolith) and Ca-P scattered inclusions of sample KS023B (uric acid). Traces of Pb were also found in all samples, sometimes along with other heavy metals such as Cr, Cd and Hg. Chromium and mercury were found only in oxalates (scattered inclusions) and uric acids, as well as arsenic and selenium. The latter was detected only in uric acid bladder stones, except for sample KS011B and the outer part of sample KS020B (Table 4). It is worth to note also the sporadic occurrence of copper in some uric acids (KS011B, KS020B and KS023B) and CaOx (KS012B).

Thermal behavior

A discrimination between anhydrous and hydrated phases occurring in the aggregates forming urinary stones is easily performed by following their thermal transformations recorded in STA analysis (Afzal et al., 1992; Basiri et al., 2012; Giannossi & Summa, 2012; Izatulina et al., 2019). The TG curve of acid uric (samples KS011B, KS020B and KS023B) shows a unique event mainly consisting in a thermal decomposition of $C_5H_4N_4O_3$ occurring in the range 300–700 °C, with a maximum decomposition rate at around 430 °C and the consequent emission of complex mixtures of carbon dioxide and other nitrile compounds (Fig. 8). TG curves also show residual masses between 1 and 3 wt.%, due to the presence of impurities such as calcium oxalate and non-stoichiometric phosphates. This information was also confirmed by FTIR analyses carried out on the residues (Suppl. Material), which showed the occurrence of calcium monoxide (sharp absorption band

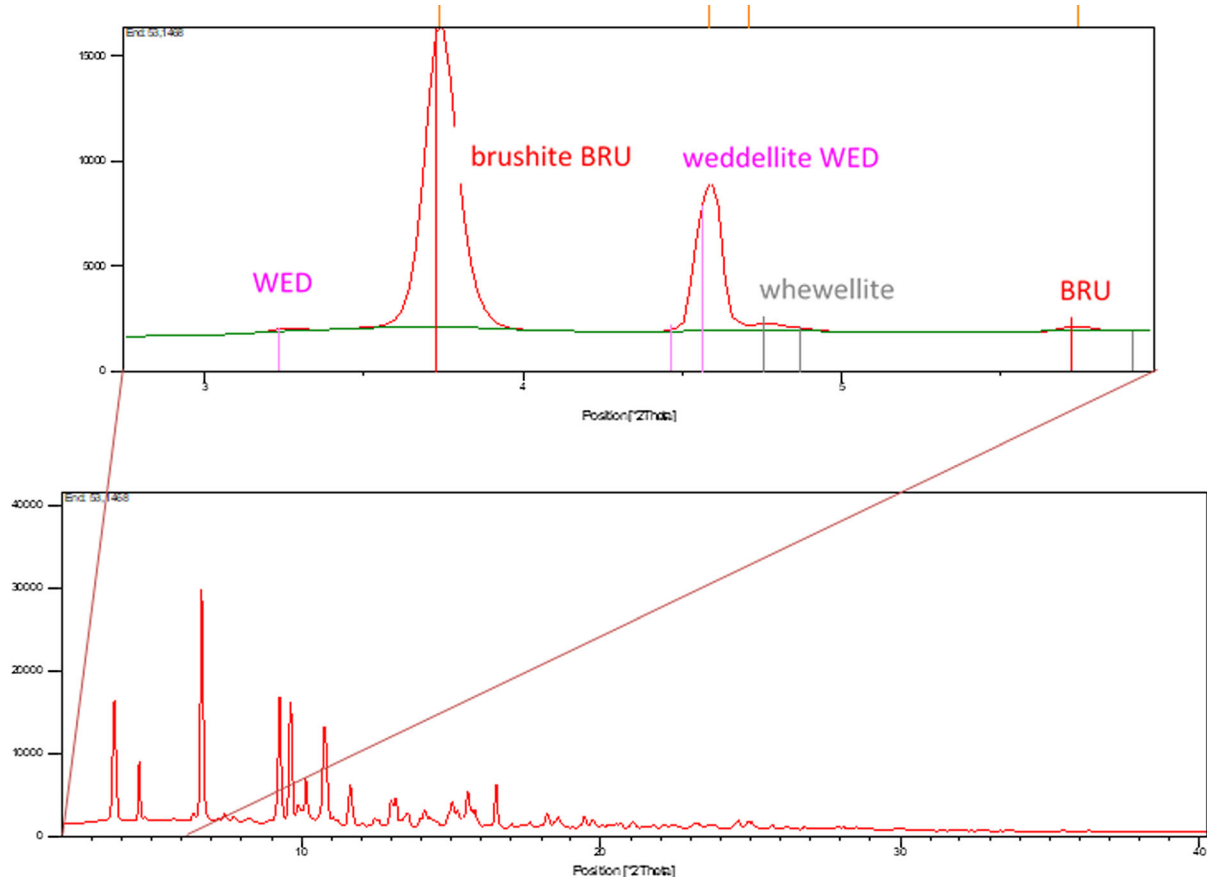

Fig. 5 X-ray diffraction pattern pertaining [2-theta (°) vs. intensity (counts)] to the sample KS006B, and zoom of the low-theta region (λ = 0.4957 Å). Red bars: brushite, purple bars: weddellite, gray bars: whewellite

at ∼ 3640 cm^{-1} and a broader one at ∼ 1410 cm^{-1}) (Berzina-Cimdina & Borodajenko, 2012; Galván-Ruiz et al., 2009) and calcium carbonate (∼ 1412, ∼ 873, and ∼ 711 cm^{-1}) (Izzo et al., 2020) as decomposition products of oxalate (Lawson-Wood & Robertson, 2016). Thermal decomposition of phosphates also accounts for the formation of hydroxyapatite (∼ 1016, ∼ 958 and ∼ 565 cm^{-1}) (Berzina-Cimdina & Borodajenko, 2012).

Thermal analyses of sample KS012B (Fig. 8) show the typical decomposition of calcium oxalate characterized by three well-defined thermal endothermic events (Lawson-Wood & Robertson, 2016). The first one is due to the dehydration of $CaC_2O_4{\cdot}H_2O$ at around 175 °C with a weight loss of ∼ 13 wt.%. During the second event (∼ 495 °C; ∼ 19.5 wt.%), the decomposition of CaC_2O_4 leads to the formation of $CaCO_3$ and the concomitant release of CO (Fig. 8). Nevertheless, as a consequence of the disproportionation reaction $2CO \rightarrow CO_2 + C$, EGA also shows the simultaneous occurrence of carbon dioxide. At ∼ 750 °C, $CaCO_3$ decomposes to form CaO and CO_2 (weight loss ∼ 29 wt.%) (Suppl. Material).

Thermal transformation of sample KS006B (Fig. 8) reflects a two-step dehydration of $CaHPO_4{\cdot}2H_2O$; the first one, within 300 °C (∼ 162 and ∼ 197 °C; weight loss ∼ 20 wt.%), forms the mineral monetite $CaHPO_4$ (Dosen & Giese, 2011; Fiore & Laviano, 1991; Jmai et al., 2019; Mulongo-Masamba et al., 2016), as well as the dehydration of oxalate impurities. Between 300–550 °C, a weight loss of about 6% indicates the complete dehydration of monetite that leads to the formation of a calcium pyrophosphate $Ca_2P_2O_7$. During this step, thermal decomposition of calcium oxalate also occurs with emission of CO and CO_2 as recorded by EGA. An additional weight loss (∼ 2.5 wt.%) between 550–800 °C, with emission of CO_2, also occurs by dissociation of calcium carbonate,

Table 4 Average concentration of major (> 1 wt.%, in bold) and trace elements (< 1wt.%) detected for bladder stones by EMPA/WDS. Main mineral species (*), standard deviation (σ), detection limits (D.L.), number of analyzed points and measurements are also reported

Sample ID	Mineral species		Ca	P	Na	K	Zn	Pb	Sr	Mg	Cr	Mn	Fe	Ni	Cu	Al	Cd	Sb	As	Se	Hg
	Brushite*	wt.%	**23.536**	**17.986**	0.063	0.034	0.109	0.057		0.024											
	(5 points)	σ	0.402	0.329		0.002	0.051	0.011		0.004											
		D.L.	0.014	0.027	0.015	0.010	0.056	0.027		0.014											
		meas.	5	5	1	3	3	2		3											
KS006B	Ca-Oxalate	wt.%	**30.954**	0.148	0.068	0.021	0.077	0.039	0.064		0.039		0.042					0.064			0.072
(16 points)	*(scattered inclusions)*	σ	0.350	0.013	0.027	0.006		0.036					0.017					0.015			
	(5 points)	D.L.	0.014	0.021	0.015	0.010	0.052	0.029	0.035		0.028		0.025					0.043			0.068
		meas.	5	5	4	4	1	2	1		1		2					3			1
	Ca-Phosphate	wt.%	**32.253**	**17.472**	0.764	0.186	0.236	0.037	0.063	0.505		0.033	0.042			0.030	0.045	0.058			
	(spheroidal particles)	σ	0.556	0.412	0.144	0.013	0.064	0.002		0.047		0.007	0.018			0.007	0.008				
	(6 points)	D.L.	0.015	0.026	0.019	0.011	0.057	0.030	0.046	0.015		0.027	0.027			0.014	0.030	0.045			
		meas.	6	6	6	6	5	2	1	6		2	2			2	2	1			
	Uric acid*	wt.%	0.031	0.034	0.033	0.023	0.043	0.038		0.017		0.020	0.019		0.041	0.015	0.040				0.086
	(5 points)	σ	0.025		0.012	0.007		0.019		0.009			0.010				0.001				
		D.L.	0.008	0.017	0.013	0.007	0.037	0.021		0.012		0.017	0.018		0.026	0.010	0.023				0.050
		meas.	4	1	3	5	1	2		2		1	2		1	1	2				1
KS011B	Ca-Oxalate	wt.%	**29.162**	0.161	0.170	0.026	0.057	0.032	0.172	0.028			0.042			0.057	0.041	0.044	0.040		
(17 points)	*(layer)*	σ	1.029	0.027	0.040	0.006	0.001		0.030	0.015						0.060					
	(6 points)	D.L.	0.014	0.021	0.016	0.010	0.051	0.029	0.052	0.013			0.026			0.013	0.031	0.043	0.034		
		meas.	6	6	6	5	2	1	2	4			1			3	1	1	1		
	Ca-Oxalate	wt.%	**28.675**	0.171	0.157	0.020	0.066	0.039		0.017		0.032	0.041			0.032					
	(scattered inclusions)	σ	0.583	0.020	0.020	0.006	0.010			0.003		0.005				0.032					
	(6 points)	D.L.	0.014	0.021	0.018	0.010	0.054	0.027		0.014		0.023	0.025			0.013					
		meas.	6	6	6	6	3	1		4		2	1			3					
	Ca-Oxalate*	wt.%	**30.228**	0.384	0.101	0.035	0.084	0.035	0.131	0.035	0.043	0.026	0.034	0.030	0.051	0.034	0.048	0.067			
	(19 points)	σ	0.929	0.120	0.028	0.014	0.019	0.007	0.051	0.018	0.010		0.006	0.001	0.016	0.014		0.006			
		D.L.	0.014	0.022	0.017	0.010	0.050	0.030	0.056	0.013	0.027	0.023	0.026	0.029	0.039	0.012	0.028	0.042			
KS012B		meas.	19		19	19	7	4	4	16	3	1	4	3	3	12	1	2			
(22 points)	Ca-Phosphate	wt.%	**33.827**	**15.697**	0.852	0.185	0.203	0.112	0.105	0.409				0.036							
	(scattered inclusions)	σ	2.164	2.735	0.068	0.011	0.013			0.009				0.004							
	(3 points)	D.L.	0.015	0.027	0.022	0.011	0.059	0.030	0.054	0.015				0.033							
		meas.	3	3	3	3	3	1	1	3				2							

Table 4 continued

	Uric acid*	wt.%	0.054	0.020	0.212	0.130	0.043	0.041	0.097	0.029					0.038	0.038					
	(outer part)	σ	0.027	0.002	0.045	0.021										0.025					
	(4 points)	D.L.	0.009	0.019	0.015	0.007	0.036	0.023	0.050	0.011					0.028	0.011					
KS020B		meas.	4	2	4	4	1	1	1	1					1	3					
(12 points)	Uric acid*	wt.%	0.018	0.023	0.033	0.033	0.056	0.052	0.085	0.014	0.034	0.018			0.041	0.04	0.026	0.029	0.039	0.041	0.099
	(inner part)	σ	0.004	0	0.009	0.012	0.006		0.027	0.004						0.009					0.003
	(8 points)	D.L.	0.008	0.017	0.016	0.007	0.036	0.020	0.041	0.011	0.019	0.017			0.026	0.010	0.022	0.027	0.026	0.021	0.048
		meas.	8	2	4	8	2	1	2	2	1	1			1	4	1	1	1	1	2
	Uric acid*	wt.%	0.024	0.027	0.028	0.024	0.064	0.034	0.084	0.015	0.026	0.019	0.018			0.043	0.027			0.029	0.061
	(11 points)	σ	0.007	0.006	0.009	0.006	0.035	0.009	0.027	0.005	0.002					0.037	0.006				0.005
		D.L.	0.009	0.018	0.015	0.008	0.038	0.021	0.046	0.010	0.019	0.017	0.017			0.010	0.023			0.023	0.052
KS022B		meas.	11	4	7	11	2	3	3	4	2	1	1			3	2			1	3
(13 points)	Ca-Oxalate	wt.%	**30.22**	0.246	0.161	0.02	0.116			0.025	0.029		0.042			0.067					
	(scattered inclusions)	σ	1.329	0.064	0.001	0.006	0.014			0.005											
	(2 points)	D.L.	0.014	0.023	0.017	0.010	0.048			0.014	0.028		0.026			0.012					
		meas.	2	2	2	2	2			2	1		1			1					
	Uric acid*	wt.%	0.021	0.025	0.021	0.035	0.039	0.046	0.094	0.013	0.031	0.021			0.035			0.043	0.027	0.03	0.084
	(6 points)	σ	0.004		0.004	0.02			0.005			0.005							0.013		
		D.L.	0.008	0.017	0.015	0.007	0.033	0.021	0.050	0.010	0.019	0.017			0.026			0.028	0.030	0.026	0.054
		meas.	5	1	4	6	1	1	2	1	1	2			1			1	2	1	1
KS023B	Ca-Oxalate	wt.%	**29.272**	0.407	0.092	0.016	0.051	0.035	0.064	0.025			0.041		0.041	0.022		0.033			0.081
(13 points)	*(scattered inclusions)*	σ	10.023	0.144	0.02	0.002				0.009			0.01								
	(5 points)	D.L.	0.014	0.020	0.016	0.010	0.041	0.030	0.046	0.013			0.024		0.032	0.011		0.032			0.079
		meas.	5	5	5	3	1	1	1	5			3		1	1		1			1
	Ca-Phosphate	wt.%	**17.895**	**9.055**	0.737	0.076	0.181	0.067	0.074	0.168		0.023	0.61	0.026		0.042	0.037				
	(scattered inclusions)	σ	11.773	6.682	0.456	0.007	0.022			0.108			0.31								
	(2 points)	D.L.	0.012	0.025	0.021	0.008	0.055	0.030	0.061	0.015		0.019	0.026	0.024		0.013	0.028				
		meas.	2	2	2	2	2	1	1	2		1	2	1		1	1				

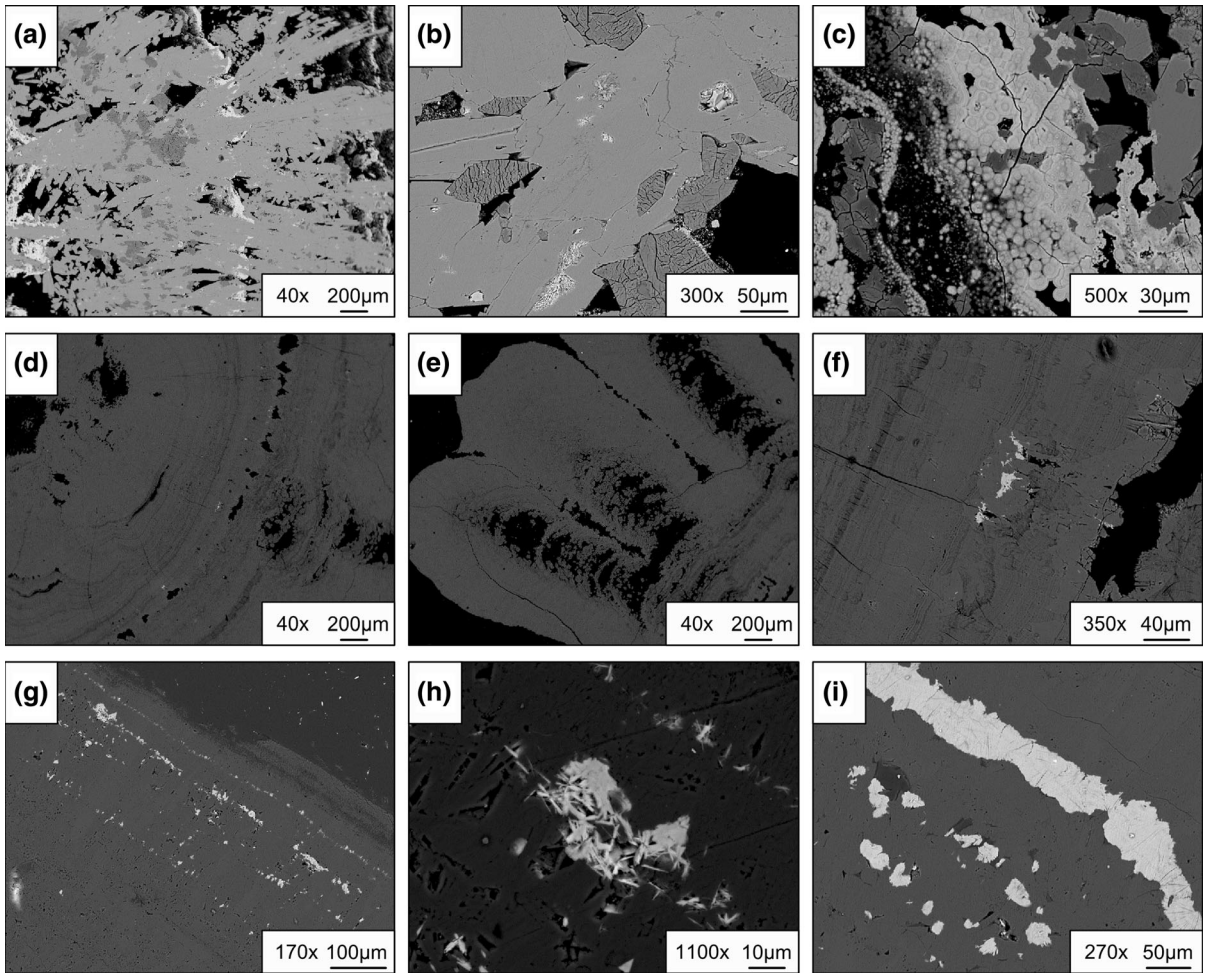

Fig. 6 Back-scattered electron (BSE) images showing the textures of the analyzed bladder stones: **a** acicular and radiating crystals of brushite, **b** bipyramidal crystals of CaOx and **c** CaP spheroidal particles in sample KS006B; **d**, **e** internal microstructure and **f** CaP inclusions for sample KS012B; **g** and **h** CaP inclusions in uric acid bladder stone (KS023B); **i** CaOx layer in KS011B (uric acid)

previously formed by decomposition of calcium oxalate. The presence of oxalate impurities along with monetite and calcium pyrophosphate was ascertained by means of FTIR analyses carried out on the residues after each thermal treatment (Suppl. Material).

Discussion

Morpho-constitutional classification

The chemical and mineralogical composition, coupled with the petrographic features, of urinary calculus allows to trace a classification on a morpho-constitutional basis, usually correlated to the specific pathophysiological conditions responsible for urolithiasis (Cloutier et al., 2015; Daudon et al., 2016; Grases et al., 1998), essential to choice the best therapeutic strategy (Frassetto & Kohlstadt, 2011; Christian Türk et al., 2016; Wang et al., 2016). Following the classification proposed by Daudon et al. (2016), further subgroups can be distinguished by a morphological observation of the surface of the stone: aspect of the section, characteristics of the *nuclei*, presence of Randall plaque, etc. Excluding the minor amounts of calcium oxalate inclusions and non-stoichiometric phosphate species detected (Tables 3, 4 and Fig. 6),

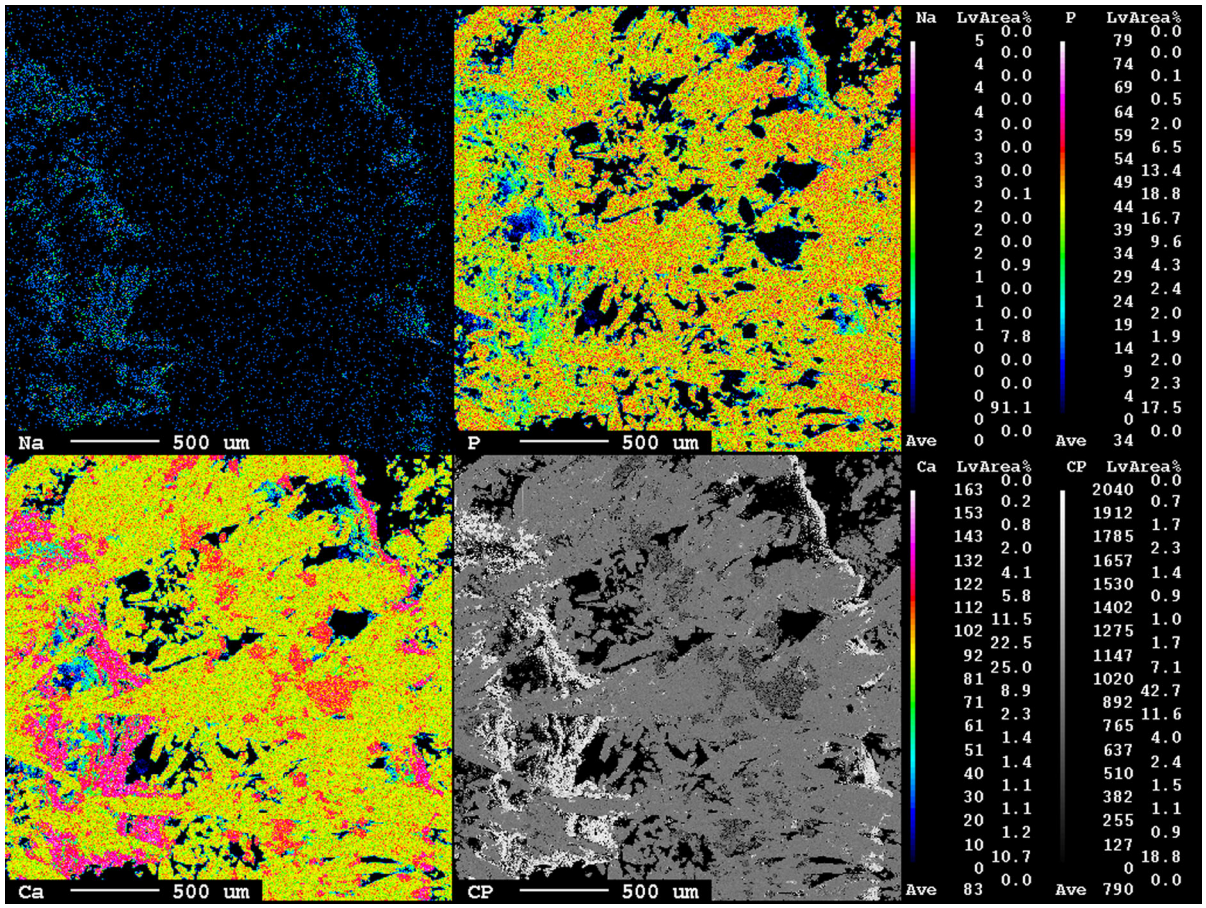

Fig. 7 Sodium, phosphorus and calcium distribution in bladder stone KS006B

the samples KS011B, KS020B KS022B, KS023B belong to the Type III (uric acids), while the KS006B and KS012B belong to the Type IV (brushite) and Type Ia classes (CaOx stones), respectively.

The compact and concentric microstructure of the samples KS011B and KS023B, along with a quite smooth surface, allow to assign them to the morphological subtypes IIIa (anhydrous uric acid), usually observed for older men affected by bladder urolithiasis, especially when interested by prostate hypertrophy (Cloutier et al., 2015; Daudon et al., 2016). Sample KS011B also displays the typical orange surface due to the presence in the urine of the red pigment uricine, easily trappable in the uric acid crystals, poorly adsorbed by the surface of sample KS023B as evidenced by the lighter shade, ranging from pale yellow to whitish. The poorly organized, porous internal microstructure of KS020B accounts for the subtype IIIb (uric acid dihydrate). Lastly, sample KS022B presented at the same time an internal, concentric and compact structure (Type IIIa) and a rough surface (Type IIIb). This transition (Type IIIa—> Type IIIb) could be due to a progressive decrease of the urine pH (< 5.5) and the consequent formation of uric acid dihydrate in the external parts of the bladder stone. The formation of uric acid-based bladder stones is often associated, in addition to the reduction of pH levels in the urine and their prolonged stasis often linked to benign hypertrophy of the prostate, also to hyperuricosuria, as well as to eating and metabolic disorders (the patient KS011B suffers from diabetes) (Cloutier et al., 2015; Daudon et al., 2016). Actually, in overweight subjects, uric acid and oxalate stones are often found. According to recent

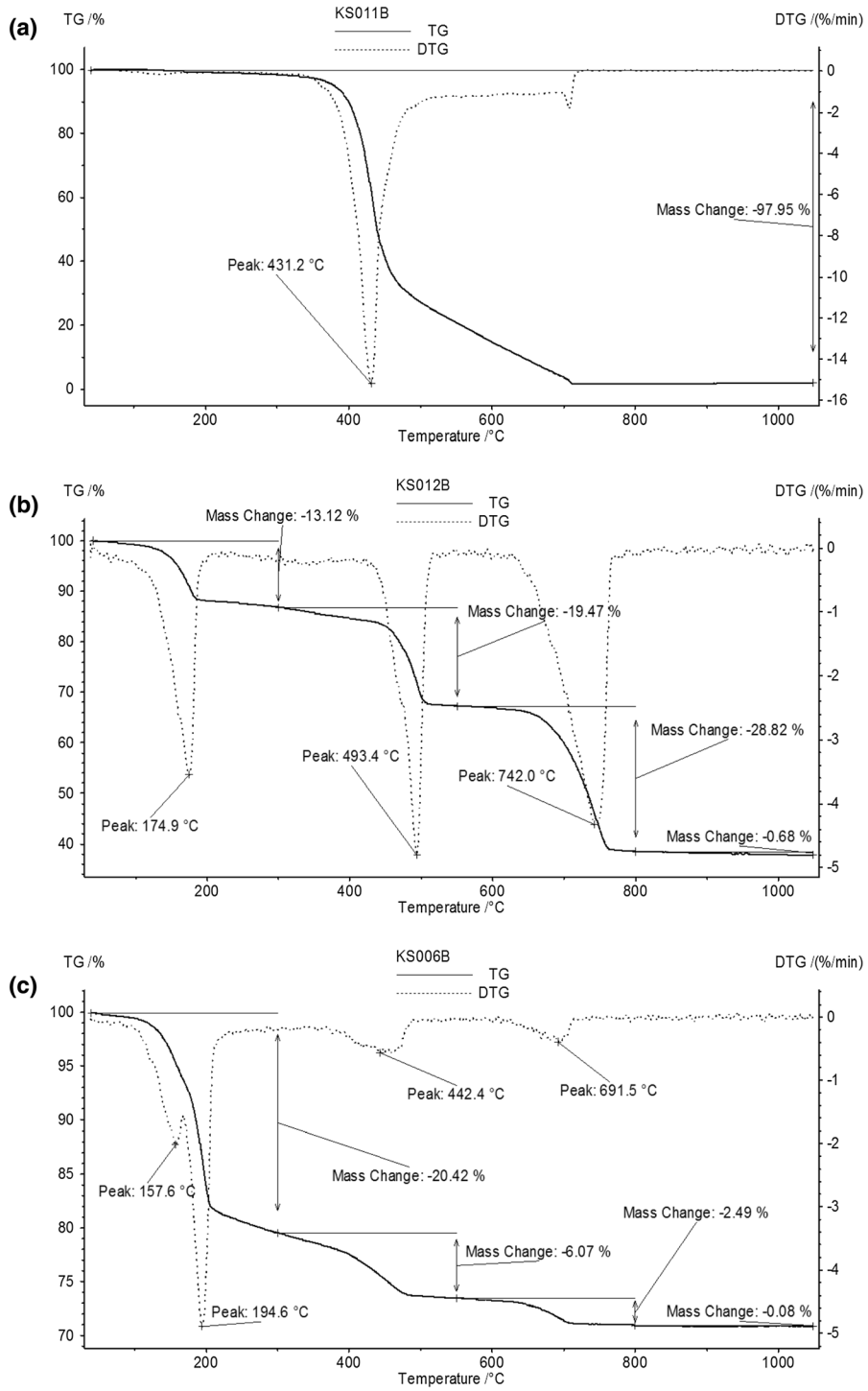

Fig. 8 Thermal analyses and EGA-FTIR of uric acid (KS011B), CaOx (KS012B) and brushite + CaOx (KS006B)

studies, there seems to be a relationship between calcium excretion and BMI. Calcium excretion could also justify the appearance of CaOx and CaP inclusions. This condition is supported in this study as all patients have a medium–high BMI index.

KS006B is a Type IVd calculus, as mainly formed by brushite and characterized by the occurrence of rod-shaped crystals arranged in a radial internal microstructure, with scarcely defined concentric patterns. Surface is rough and dappled. This kind of bladder stone is usually considered as idiopathic, namely related to unknown causes, although often observed in patients affected by primary hyperparathyroidism, hypercalciuria and medullary sponge kidney (Evan et al., 2005; Klee et al., 1991). Considering the high recurrence rate of these stones and their resistance to extracorporeal shock wave lithotripsy (ESWL), patients affected by brushite urolithiasis usually require more aggressive clinical treatments (Daudon et al., 2016). KS006B also shows the occurrence of inclusions of CaOx (mainly weddellite) and spheroidal particles of non-stoichiometric and amorphous CaP stones, located as concentric layers in the porous system of brushite aggregate. It is possible that the latter inclusions act as precursors for apatite stones and the higher content of calcium could deal with the composition of amorphous calcium phosphate and/or rarer CaP phases, indicating hypercalciuria or urinary tract infection (Daudon et al., 2016) and indicative of recent lithogenic processes (Cloutier et al., 2015). Morphological features of these spherical inclusions remind those of some common inorganic mineral concretions (i.e., ooids) generally formed in subaqueous environments. It is possible that the mechanism of formation of these inclusions was due to the interaction of supersaturated urine through the porous system of brushite, with a consequent release of calcium phosphate around a starting *nucleus* (Giannossi, 2013). The tendency to form a perfect sphere could be strictly related to kinetic energy of the urine flow and/or steric effects between CaP inclusions (Hill & Forti, 1997).

Sample KS012B shows a spiculated appearance that allow us to classify this stone among the so-called *Jackstone calculi* (Brogna et al., 2018, 2019; Goonewardena et al., 2021; Perlmutter et al., 2002; Rivell & Coren, 2012; Subasinghe et al., 2017; Sweeney & Dyer, 2015). This kind of urinary stone is freely movable in the bladder and is usually composed, according to literature (Brogna et al., 2018, 2019; Perlmutter et al., 2002), by calcium oxalate dehydrate. Considering the mineralogical composition and the poorly organized internal microstructure and the spiculated surface, sample KS012B generally accounts for Type Ia urinary stone, typical of CaOx aggregates. It is possible that calcium oxalates, initially hydrate, converted to more stable mineralogical (anhydrous) phases (Conti et al., 2010; Giannossi, 2013; Gibson, 1974).

Assumption on meaning of major and trace elements

The role of major and trace elements in the pathogenesis of urinary stones was widely investigated in the last decades, encouraging the use of these biominerals for biomonitoring purposes (Giannossi, 2010; Giannossi et al., 2013; V. K. Singh & Rai, 2014; Wang et al., 2019). In particular, major and trace elements naturally occur in biocrystals as a consequence of food intake, metabolic processes and environmental factors. However, part of the trace elements can be accidentally incorporated into urinary stones, after a temporary storage in the kidneys, and can sometimes even affect the formation of crystals, thus acting as promoter or inhibitor agents (Giannossi et al., 2013; Kuta et al., 2012; Singh & Rai, 2014).

The most relevant element for the lithogenesis of urinary stones is doubtless calcium, which occurs in the present study as major element in CaOx and CaP uroliths (either as dominant mineralogical species/minor inclusions; Table 5), or trace elements in uric acids. It is widely accepted that Ca can significantly influence the distribution of other trace elements, promoting the new crystallization processes in kidney or bladder (Basavaraj et al., 2007; Gomez et al., 2021). In calcium-bearing phases forming uroliths, this element can be partially replaced by substituent ions as sodium, magnesium or strontium, the latter particularly observed in CaOx phases. Since magnesium acts as inhibitor element in urolithiasis, its occurrence turns to be useful for the treatment and prevention of kidney stones (Frassetto & Kohlstadt, 2011).

Most of the calcium comes from Daily Dietary Intakes (DDI), especially from hard waters. Nevertheless, during the interview all the patients reported to drink mostly bottled water, except for patient KS022B (producer of uric acid stone), drinking only local tap

water. It is worth to note that the fraction of calcium in the CaOx species is particularly higher than that expected for COD (ca. 24 wt.%) or COM (ca. 27 wt.%), and mainly follows the stoichiometric composition of anhydrous calcium oxalate (namely, ca. 31 wt.%). According to literature (Bazin et al., 2016; Conti et al., 2010; Giannossi, 2013; Gibson, 1974; Zhao et al., 2016), whewellite is the most common and stable calcium oxalate that can be formed by partial dehydration of weddellite. This process could give rise to a perfect pseudomorphism (Gibson, 1974), as observable for bipyramidal crystal inclusions in brushite aggregate KS006B. It is possible that oxalates in bladder stones can evolve to more stable (i.e., more anhydrous) phases, probably thanks to the dry conditions allowed by the internal and more compact parts of these aggregates, especially observed in the jackstone calculus KS012B.

Trace elements have been encountered in the CaP phases as a consequence of the isomorphic substitutions. Among them, metals such as sodium, iron, magnesium, zinc and potassium reach the highest values. The role of some of these metals in lithogenesis, for example zinc and iron, is still debated, whereas undesired trace elements such as copper, cadmium, lead, chromium, mercury and arsenic are generally attributable to environmental pollution or contaminated food. As a matter of fact, some of these elements (i.e., Hg, Cu and Cd) can cause important healthy problems, especially in kidney damage (Giannossi et al., 2013; Kuta et al., 2012; Pal'chik et al., 2006). In the present study, Pb was detected in all the examined samples and its average elemental concentration (ca. 480 ppm) is consistent with that reported in the literature for Basilicata region (southern Italy) (Giannossi et al., 2013), as well as average concentrations of Cr found both in CaOx and uricite minerals. Another dangerous element, Hg, is often observed in association with selenium and displays significantly high concentrations (on average ca. 800 ppm). Mercury is toxic also at low concentrations and can occur in environment and in food chain rarely as inorganic form (e.g., native Hg) or most commonly as organic form (mainly methylmercury or ethylmercury) (Jiang et al., 2021; Lin et al., 2021; Moser et al., 2020). The presence in the human body is also known to be ascribed to the dental amalgam restoration.

The role of selenium as inhibitor in urinary stones formation has been clearly highlighted in literature (Singh & Rai, 2014). Selenium is considered an essential trace element for human body and its simultaneous occurrence with Hg seems to be mainly attributable to a methylmercury (CH_3Hg^+) detoxification process, often leading to the formation of a rare HgSe compound known as tiemannite, recently found as small inclusion (< 10 μm) in a struvite bladder stone, surgically removed from a four-year-old Austrian patient (Moser et al., 2020). The authors detected tiemannite via EMPA and considered the conditions of crystallization of this mineral as consistent with those required for struvite precipitation, namely low temperature (ca. 25 °C) and high pH values (up to 12), quite consistent with human body temperature (Moser et al., 2020). In our investigation, Hg and Se were found in uric acid bladder stones (70/30 Hg/Se wt.% ratio) that usually form in low pH urine, also compatible with the formation of tiemannite (Hazen et al., 2012; Moser et al., 2020). Therefore, we do not exclude that Hg and Se detected in the present study could be related to the occurrence of tiemannite tiny crystals.

The amount of Cu appears significantly lower than data from literature and is mainly observed in uric acid uroliths. Lastly, according to the literature (Singh & Rai, 2014), arsenic is often associated with antimony. The latter can accumulate in the human body displacing essential elements and acting as toxin (Słojewski, 2011).

From a clinical point of view, it is possible to consider the main causes that could lead to the formation of the examined bladder stones (Table 5). Except for the sample with brushite (KS006B) which suggests an idiopathic nature (Daudon et al., 2016), for all the others it can be assumed that the cause is a condition of urine stasis due to potential obstructions of the urinary tract, favoring the considerable accumulation and consequent growth of these aggregates. Moreover, epistemological questionnaires report that patients daily consume alcohol, protein-rich (e.g., meats, eggs, cheeses) and oxalate-rich (e.g., coffee, cocoa, dried fruit) foods, all likely concurring to generate supersaturated urine which may lead to the precipitation of uric acids and calcium oxalates, especially if associated to particularly low pH values.

Conclusions

This multidisciplinary study has led to the characterization and classification of human bladder stones (including a jackstone calculus) of patients residing in the Campania region. As similar studies were not so far reported in the open-source literature, this contribution sheds new light on the potential clinical assumptions and some implications in the geohealth sphere, linked to the presence of some specific essential and non-essential heavy metals that can be trapped in the biominerals mainly replacing cations and anions in the structural sites of the lattice.

Some considerations on the most common therapies to carry out in order to mitigate the risk of urolithiasis are hereafter reported. First of all, according to the literature (Bao & Wei, 2012; Borghi et al., 1996), all stone formers should pursue correct lifestyle and dietary habits based on a regular fluid intake (2.5–3.0 L/day, mostly water) and a proper diuresis (2.0–2.5 L/day). A common-sense approach to diet should be taken: avoiding any excess, all food groups should be mixed and balanced encouraging fruit and vegetable intakes (Turney et al., 2014) and limiting the daily consumption of animal proteins (0.8–1.0 g/kg) (Dussol et al., 2008) and NaCl (3–5 g/day). A regular physical activity can contrast some lifestyle factors that may influence the risk of stone formation such as obesity (Siener et al., 2004) and arterial hypertension (Madore et al., 1998).

Apart from these general recommendations, prevention and treatment of urolithiasis could be strictly related to the stone type (Frassetto & Kohlstadt, 2011). For example, the recurrence of CaOx (KS012B patient) and uric acids (KS011B, KS020B, KS022B and KS023B patients) could be solved increasing pH of urines with alkaline-rich food (i.e., citrate supplementation, fruit and vegetable intakes, alkaline mineral waters, etc.). Intake of purine-rich food should be restricted in patients with hyperuricosuric calcium oxalate and uric acid stones (Coe, 1978), the daily intake should not exceed 500 mg. Calcium should not be restricted for CaOx formers but limited to 1.0–1.2 g/day (Curhan et al., 1997). As far as phosphate stone formers (KS006B patient) are concerned urine acidification using, for example, cranberry juice or betaine is recommended. For all these reasons, a detailed mineralogical characterization of urinary stones should be always required for well-defining a good therapeutical approach. A brand-new finding worth to be underlined is that the distribution of the investigated chemical elements was regulated by each single mineralogical species that contributes to the urinary stones' formation. This leads us to believe that an evaluation of the type and content of major and trace elements can not be only achieved by means of wet chemical analysis (i.e., bulk chemical analysis). Actually, these techniques (e.g., Atomic Absorption Spectroscopy, AAS; Inductively Coupled Plasma, ICP) require a total destruction of the sample by

Table 5 Synoptic table reporting classification of bladder stones examined in the present study and main clinical assumption

n	ID_sample	Type*	Dominant phases	Minor Phases	Undesired elements	Clinical assumption*
1	KS006B	IVd	Brushite	CaOx, CaP	Hg, Pb, Sb, Cd, Cr	Idiopathic, potential exposure to pollution
2	KS011B	IIIa	Uric acid	CaOx	Hg, As, Pb, Sb, Cd, Cu	Eating and metabolic disorders, stasis, hyperuricosuria, hypercalciluria, potential exposure to pollution
3	KS012B	Ia	CaOx	CaP	Pb, Cd, Sb, Cu, Cr,	Hyperoxaluria, hypercalciluria, stasis, potential exposure to pollution
4	KS020B	IIIb	Uric acid	–	Hg, Pb, As, Se, Cd, Cu, Cr	Stasis, hyperuricosuria, potential exposure to pollution
5	KS022B	IIIa/ IIIb	Uric acid	CaOx	Hg, Pb, Se, Cd, Cr	Stasis, low urine pH, hyperuricosuria, hypercalciluria, potential exposure to pollution
6	KS023B	IIIa	Uric acid	CaOx, CaP	Hg, Pb, As, Se, Cd, Cu, Cr	Stasis, hyperuricosuria, hypercalciluria, potential exposure to pollution

*, *according to Daudon* et al. 2016*, and Cloutier et al.* 2015

digestion and provide chemical data representative of the entire stone sample. By contrast, the use of microscopic techniques coupled with microanalysis, such as those used for this study (i.e., EMPA/WDS) or others (e.g., LA-ICP-MS) (Chaudhri et al., 2007), allows to investigate the sample, without destroying it, in a short time and with an acceptable limits of detection. The added value to our scientific and analytical approach is that we can discriminate the mineralogical species where these elements tend to concentrate, for example by isomorphic substitution. Table 4 shows the concentrations of the investigated elements (Na, K, Mg, Ca, Sr, Cr, Mn, Fe, Ni, Cu, Zn, Cd, Hg, Al, Sb, Pb, As, Se, P) in each mineralogical species of each sample. Excluding the most abundant elements (mainly Ca and P), all the others occur in the range of about one percent in weight. There is, therefore, a dualism in the partitioning of the elements in the mineralogical species belonging to the investigated urinary stones. The clearest interpretation is to consider calcium and phosphorus as the elements generating inorganic bladder stones, coming from the DDI and influencing the distribution of all the others trace elements. The concentrations of trace elements as a function of DDI have been addressed in several papers (Giannossi et al., 2013 and references therein). Some are related to studies carried out on sedentary populations (e.g., Iran, Jordan) (Abboud, 2008; Keshavarzi et al., 2015), which therefore return a fairly realistic representation of the contamination induced by the ingestion of food mostly consisting of ingredients (water, milk and dairy, vegetables, meat, etc.) from the areas where they live. In contrast, a very different situation occurs in Western populations, like the one resident in the Campania region, where food is not derived from local production processes, and, thus, infinite variables do not allow to univocally associate anomalous concentrations of trace elements to the territory in which the patient lives. In this study, the clinical interviews clearly indicate that the majority of patients drink bottled water and wine, the origin of which are unknown, and probably ascribable to areas far from their residence. At present, it is therefore not possible to make robust correlations between the geological environment hosting the patient and the presence of essential (Cr, As, Cu and Se) and non-essential heavy metals (Hg, Pb, Cd, Sb). Nevertheless, excluding the ingestion of food contaminated by these undesired elements, a careful attention should be paid to the reduction of some environmental risk factors such as the exposure to the use of fertilizers (in agreement with the main working activity of the investigated patients), the handling of chemical substances, varnishes, pigments and metals (Ferguson, 1990). On these basis, it is necessary to promote further studies that take into consideration a wider set of urinary stones (bladder, kidney stones) and consequently, of patients in order to increase the number of cases necessary to provide a statistically robust research. Above all, the combined use of wet chemical analysis (AAS, ICP) and EMPA/WDS must be envisaged for the purposes of dosing the trace elements and to satisfy two requests: how much is there and where the element is going to be concentrated.

Finally, the involvement of further expertise such as physiologists and nephrologists will be able to dispel the uncertainty regarding the possibility of understanding the mechanisms of biominerogenesis and the way and timing of accumulation of essential and non-essential heavy metals during the nucleation and growth of this impacting biominerals.

Acknowledgements ELETTRA Sincrotrone Trieste is thanked for the allocation of the beam-time, and Paolo Lotti for the assistance during the XRD data collection. Andrea Risplendente is thanked for the assistance during the EMPA/WDS analysis. The authors also thank: Antonia Cinelli and Valentina Materazzo for their collaboration in the first steps of the present investigation; Prof. Vincenzo Morra and Prof. Piergiulio Cappelletti for early discussions; Paolo Dello Russo (LITHOS lab) for helping us to prepare the thin sections.; the two anonymous referees for their precious and important suggestions which largely improved the manuscript. Lastly, the present investigation was carried out with the financial support of University of Sannio Benevento (Department of Science and Technology) research funding (FRA 2020 granted to dr. Mariano Mercurio).

Authors' contribution All the authors critically contributed to the writing and editing of manuscript draft, investigation, analysis and interpretation of data. The authors also approved the final version of the manuscript to be submitted for publication.

Funding This work was supported by Department of Science and Technology University of Sannio Benevento (FRA2020 granted to Mariano Mercurio).

Availability of data and material All data are included in the present manuscript. Further information can be request to the corresponding author.

Declarations

Conflict of interest The authors have no conflicts of interest to declare that are relevant to the content of this article.

Human research/Consent to Participate/Consent to Publish Clinical interviews were held in anonymous form. All patients consent to participate at present investigation and to publish the data in a journal article.

References

Abboud, I. A. (2008). Mineralogy and chemistry of urinary stones: Patients from North Jordan. *Environmental Geochemistry and Health, 30*, 445–463. https://doi.org/10.1007/s10653-007-9128-7

Abrol, N., & Kekre, N. S. (2014). Revisiting Randall's plaque. *African Journal of Urology, 20*, 174–179. https://doi.org/10.1016/j.afju.2014.06.001

Afaj, A. H., & Sultan, M. A. (2005). Mineralogical composition of the urinary stones from different provinces in Iraq. *TheScientificWorldJOURNAL, 5*, 24–38. https://doi.org/10.1100/tsw.2005.2

Afzal, M., Iqbal, M., & Ahmad, H. (1992). Thermal analysis of renal stones. *Journal of Thermal Analysis, 38*, 1671–1682. https://doi.org/10.1007/BF01979363

Ancharov, A. I., Potapov, S. S., Moiseenko, T. N., Feofilov, I. V., & Nizovskii, A. I. (2007). Model experiment of in vivo synchrotron X-ray diffraction of human kidney stones. *Nuclear Instruments and Methods in Physics Research Section A: Accelerators, Spectrometers, Detectors and Associated Equipment, 575*(1–2), 221–224.

Ansari, M. S., & Gupta, N. P. (2003). Impact of socioeconomic status in etiology and management of urinary stone disease. *Urologia Internationalis, 70*(4), 255–261. https://doi.org/10.1159/000070130

Aslin Shamema, A., Thanigai Arul, K., Senthil Kumar, R., & Kalkura, S. N. (2015). Physicochemical analysis of urinary stones from Dharmapuri district. *Spectrochimica Acta - Part A: Molecular and Biomolecular Spectroscopy, 134*, 442–448. https://doi.org/10.1016/j.saa.2014.05.088

Brogna, B., Flammia, F., Flammia, F. C., & Flammia, U. (2019). Jackstone calculus: A rare subtype of urinary stone with a sea-urchin appearance. *International Journal of Nephrology and Kidney Failure, 4*(5), 1–2. https://doi.org/10.16966/2380-5498.166

Bao, Y., & Wei, Q. (2012). Water for preventing urinary stones. Cochrane database of systematic reviews. *Cochrane Database Systematic Review, 2*(2), CD004292. https://doi.org/10.1002/14651858.CD004292.pub3

Basavaraj, D. R., Biyani, C. S., Browning, A. J., & Cartledge, J. J. (2007). The role of urinary kidney stone inhibitors and promoters in the pathogenesis of calcium containing renal stones {A figure is presented}. *EAU-EBU Update Series, 5*, 126–136. https://doi.org/10.1016/j.eeus.2007.03.002

Basiri, A., Taheri, M., & Taheri, F. (2012). What is the state of the stone analysis techniques in urolithiasis? *Urology Journal, 9*(2), 445–454. https://doi.org/10.22037/uj.v9i2.1469

Bazin, D., Leroy, C., Tielens, F., Bonhomme, C., Bonhomme-Coury, L., Damay, F., et al. (2016). Hyperoxaluria is related to whewellite and hypercalciuria to weddellite: What happens when crystalline conversion occurs? *Comptes Rendus Chimie, 19*(11–12), 1492–1503.

Berzina-Cimdina, L., & Borodajenko, N. (2012). Research of calcium phosphates using fourier transform infrared spectroscopy. In *Infrared Spectroscopy - Materials Science, Engineering and Technology* (pp. 123–148). Doi: https://doi.org/10.5772/36942

Borghi, L., Meschi, T., Amato, F., Briganti, A., Novarini, A., & Giannini, A. (1996). Urinary volume, water and recurrences in idiopathic calcium nephrolithiasis: A 5-year randomized prospective study. *The Journal of Urology, 155*(3), 839–843.

Brogna, B., Flammia, F., Flammia, F. C., & Flammia, U. (2018). A large jackstone calculus incidentally detected on ct examination: A case report with literature review. *World Journal of Nephrology and Urology, 7*(3–4), 85–87. https://doi.org/10.14740/wjnu372

Chatterjee, P., Chakraborty, A., & Mukherjee, A. K. (2018). Phase composition and morphological characterization of human kidney stones using IR spectroscopy, scanning electron microscopy and X-ray Rietveld analysis. *Spectrochimica Acta - Part A: Molecular and Biomolecular Spectroscopy, 200*, 33–42. https://doi.org/10.1016/j.saa.2018.04.005

Chaudhri, M. A., Watling, J., & Khan, F. A. (2007). Spatial distribution of major and trace elements in bladder and kidney stones. *Journal of Radioanalytical and Nuclear Chemistry, 271*(3), 713–720.

Çiftçioğlu, N., Vejdani, K., Lee, O., Mathew, G., Aho, K. M., Kajander, E. O., et al. (2008). Association between Randall's plaque and calcifying nanoparticles. *International Journal of Nanomedicine, 3*(1), 105.

Cloutier, J., Villa, L., Traxer, O., & Daudon, M. (2015). Kidney stone analysis: "Give me your stone, I will tell you who you are!" *World Journal of Urology, 33*, 157–169. https://doi.org/10.1007/s00345-014-1444-9

Coe, F. L. (1978). Hyperuricosuric calcium oxalate nephrolithiasis. *Kidney International, 13*(5), 418–426. https://doi.org/10.1038/ki.1978.60

Conti, C., Brambilla, L., Colombo, C., Dellasega, D., Gatta, G. D., Realini, M., & Zerbi, G. (2010). Stability and transformation mechanism of weddellite nanocrystals studied by X-ray diffraction and infrared spectroscopy. *Physical Chemistry Chemical Physics, 12*, 14560–14566. https://doi.org/10.1039/c0cp00624f

Curhan, G. C., Willett, W. C., Rimm, E. B., Speizer, F. E., & Stampfer, M. J. (1998). Body size and risk of kidney stones. *Journal of the American Society of Nephrology, 9*(9), 1645–1652.

Curhan, G. C., Willett, W. C., Speizer, F. E., Spiegelman, D., & Stampfer, M. J. (1997). Comparison of dietary calcium with supplemental calcium and other nutrients as factors affecting the risk for kidney stones in women. *Annals of Internal Medicine, 126*(7), 497–504. https://doi.org/10.7326/0003-4819-126-7-199704010-00001

Daudon, M., Dessombz, A., Frochot, V., Letavernier, E., Haymann, J. P., Jungers, P., & Bazin, D. (2016). Comprehensive morpho-constitutional analysis of urinary stones improves etiological diagnosis and therapeutic strategy of nephrolithiasis. *Comptes Rendus Chimie, 19*, 1470–1491. https://doi.org/10.1016/j.crci.2016.05.008

Dosen, A., & Giese, R. F. (2011). Thermal decomposition of brushite, CaHPO4·2H2O to monetite CaHPO4 and the formation of an amorphous phase. *American Mineralogist, 96*, 368–373. https://doi.org/10.2138/am.2011.3544

Dussol, B., Iovanna, C., Rotily, M., Morange, S., Leonetti, F., Dupuy, P., et al. (2008). A randomized trial of low-animal-protein or high-fiber diets for secondary prevention of calcium nephrolithiasis. *Nephron Clinical Practice, 110*(3), c185–c194.

Evan, A. P., Lingeman, J. E., Coe, F. L., Shao, Y., Parks, J. H., Bledsoe, S. B., et al. (2005). Crystal-associated nephropathy in patients with brushite nephrolithiasis. *Kidney International, 67*(2), 576–591. https://doi.org/10.1111/j.1523-1755.2005.67114.x

Ferguson, J. E. (1990). *The heavy elements: Chemistry, environmental impact and health effects*. Pergamon Press.

Fiore, S., & Laviano, R. (1991). Brushite, hydroxylapatite, and taranakite from Apulian caves (southern Italy): New mineralogical data. *American Mineralogist, 76*(9–10), 1722–1727.

Frassetto, L., & Kohlstadt, I. (2011). Treatment and prevention of kidney stones: An update. *American Family Physician, 84*(11), 1234–1242.

Galván-Ruiz, M., Hernández, J., Baños, L., Noriega-Montes, J., & Rodríguez-García, M. E. (2009). Characterization of Calcium carbonate, calcium oxide, and calcium hydroxide as starting point to the improvement of lime for their use in construction. *Journal of Materials in Civil Engineering, Do*. https://doi.org/10.1061/(ASCE)0899-1561(2009)21:11(694)

Giannossi, M. L., & Summa, V. (2012). A Review of Pathological Biomineral Analysis Techniques and Classification Schemes. In A. Cumhur (Ed.), *An Introduction to the Study of Mineralogy* (pp. 123–146). Doi: https://doi.org/10.5772/34861

Giannossi, M. L. (2013). *Studio di biominerali patologici presenti nel corpo umano: caratteri composizionali ed influenza ambientale nel caso studio della Basilicata*. Consiglio Regionale della Basilicata.

Giannossi, M. L. (2010). La geologia in difesa della salute: Nuovi sbocchi professionali. *Geologia Territorio Ambiente, 7*, 3–9.

Giannossi, M. L., Mongelli, G., Tateo, F., & Summa, V. (2012). Mineralogical and morphological investigation of kidney stones of a Mediterranean region (Basilicata, Italy). *Journal of X-Ray Science and Technology, 20*(2), 175–186.

Giannossi, M. L., Summa, V., & Mongelli, G. (2013). Trace element investigations in urinary stones: A preliminary pilot case in Basilicata (Southern Italy). *Journal of Trace Elements in Medicine and Biology, 27*, 91–97. https://doi.org/10.1016/j.jtemb.2012.09.004

Gibson, R. I. (1974). Descriptive human pathological mineralogy. *American Mineralogist: Journal of Earth and Planetary Materials, 59*(11–12), 1177–1182.

Gomez, A., Narayan, M., Zhao, L., Jia, X., Bernal, R. A., Lopez-Moreno, M. L., & Peralta-Videa, J. R. (2021). Effects of nano-enabled agricultural strategies on food quality: Current knowledge and future research needs. *Journal of Hazardous Materials, 401*, 123385. https://doi.org/10.1016/j.jhazmat.2020.123385

Goonewardena, S., Jayarajah, U., Kuruppu, S. N., & Fernando, M. H. (2021). Jackstone in the kidney: An unusual calculus. *Case Reports in Urology*. https://doi.org/10.1155/2021/8816547

Gràcia-Garcia, S., Millán-Rodríguez, F., Rousaud-Barón, F., Montañés-Bermúdez, R., Angerri-Feu, O., Sánchez-Martín, F., et al. (2011). Why and how we must analyze urinary calculi. *Actas Urológicas Españolas, 35*(6), 354–362. https://doi.org/10.1016/j.acuroe.2011.01.005

Grases, F., Costa-Bauzá, A., & García-Ferragut, L. (1998). Biopathological crystallization: a general view about the mechanisms of renal stone formation. *Advances in Colloid and Interface Science, 74*(1), 169–194. https://doi.org/10.1016/S0001-8686(97)00041-9

Hammersley, A. P. (2016). FIT2D: A multi-purpose data reduction, analysis and visualization program. *Journal of Applied Crystallography, 49*, 646–652. https://doi.org/10.1107/S1600576716000455

Hazen, R. M., Golden, J., Downs, R. T., Hystad, G., Grew, E. S., Azzolini, D., & Sverjensky, D. A. (2012). Mercury (Hg) mineral evolution: A mineralogical record of supercontinent assembly, changing ocean geochemistry, and the emerging terrestrial biosphere. *American Mineralogist, 97*(7), 1013–1042.

Hill, C., & Forti, P. (1997). *Cave minerals of the world* (2nd ed.). National Speleological Society.

Hirsch, A., Azuri, I., Addadi, L., Weiner, S., Yang, K., Curtarolo, S., & Kronik, L. (2014). Infrared absorption spectrum of brushite from first principles. *Chemistry of Materials, 26*(9), 2934–2942. https://doi.org/10.1021/cm500650t

Hornberger, B., & Bollner, M. R. (2018). Kidney stones. *Physician Assistant Clinics, 3*(1), 37–54.

Izatulina, A. R., Gurzhiy, V. V., Krzhizhanovskaya, M. G., Chukanov, N. V., & Panikorovskii, T. L. (2019). Thermal behavior and phase transition of uric acid and its dihydrate form, the common biominerals uricite and tinnunculite. *Minerals, 9*, 373. https://doi.org/10.3390/min9060373

Izzo, F., Germinario, C., Grifa, C., Langella, A., & Mercurio, M. (2020). External reflectance FTIR dataset (4000–400 cm^{-1}) for the identification of relevant mineralogical phases forming Cultural Heritage materials. *Infrared Physics and Technology, 106*, 103266. https://doi.org/10.1016/j.infrared.2020.103266

Jiang, L., Zhang, R., Zhang, L., Zheng, R., & Zhong, M. (2021). Improving the regulatory health risk assessment of mercury-contaminated sites. *Journal of Hazardous Materials, 402*, 123493. https://doi.org/10.1016/j.jhazmat.2020.123493

Jmai, S., Bagane, M., & Queneudec-T'kint, M. (2019). Physico-chemical, thermal, thermodynamic and kinetic characterization of a porous material (Di-calcium phosphate). *Heat and Mass Transfer/waerme- Und Stoffuebertragung, 55*, 3589–3602. https://doi.org/10.1007/s00231-019-02625-x

Kanchana, G., Sundaramoorthi, P., & Jeyanthi, G. P. (2009). Bio-chemical analysis and FTIR-spectral studies of artificially removed renal stone mineral constituents. *Journal of Minerals and Materials Characterization and Engineering, 8*(2), 161–170. https://doi.org/10.4236/jmmce.2009.82014

Keshavarzi, B., Ashayeri, N. Y., Moore, F., Irani, D., Asadi, S., Zarasvandi, A., & Salari, M. (2016). Mineralogical composition of urinary stones and their frequency in patients: Relationship to gender and age. *Minerals, 6*, 131. https://doi.org/10.3390/min6040131

Keshavarzi, B., Yavarashayeri, N., Irani, D., Moore, F., Zarasvandi, A., & Salari, M. (2015). Trace elements in urinary stones: A preliminary investigation in Fars province, Iran. *Environmental Geochemistry and Health, 37*, 377–389. https://doi.org/10.1007/s10653-014-9654-z

Klee, L. W., Brito, C. G., & Lingeman, J. E. (1991). The clinical implications of brushite calculi. *Journal of Urology, 145*(4), 715–718. https://doi.org/10.1016/S0022-5347(17)38432-X

Kumar, V., Farell, G., Yu, S., Harrington, S., Fitzpatrick, L., Rzewuska, E., et al. (2006). Cell biology of pathologic renal calcification: Contribution of crystal transcytosis, cell-mediated calcification, and nanoparticles. *Journal of Investigative Medicine, 54*(7), 412–424.

Kuta, J., Machát, J., Benová, D., Červenka, R., & Kořistková, T. (2012). Urinary calculi: Atypical source of information on mercury in human biomonitoring. *Central European Journal of Chemistry, 10*(5), 1475–1483. https://doi.org/10.2478/s11532-012-0063-9

Kuta, J., Machát, J., Benová, D., Červenka, R., Zeman, J., & Martinec, P. (2013). Association of minor and trace elements with mineralogical constituents of urinary stones: A hard nut to crack in existing studies of urolithiasis. *Environmental Geochemistry and Health, 35*(4), 511–522.

Lawson-Wood, K., & Robertson, I. (2016). Study of the Decomposition of Calcium Oxalate Monohydrate using a Hyphenated Thermogravimetric Analyser - FT-IR System (TG-IR). Seer Green, England: PerkinElmer, Inc. https://www.perkinelmer.com/lab-solutions/resources/docs/APP_Decomposition_Calcium Oxalate_Monohydrate(013078_01).pdf

Le Bail, A., Duroy, H., & Fourquet, J. L. (1988). Ab-initio structure determination of LiSbWO6 by X-ray powder diffraction. *Materials Research Bulletin, 23*(3), 447–452. https://doi.org/10.1016/0025-5408(88)90019-0

Letavernier, E., Bazin, D., & Daudon, M. (2016). Randall's plaque and kidney stones: Recent advances and future challenges. *Comptes Rendus Chimie, 19*, 1456–1460. https://doi.org/10.1016/j.crci.2014.12.005

Li, X., Zhao, R., Liu, B., & Yu, Y. (2013). Gemstone spectral imaging dual-energy computed tomography: A novel technique to determine urinary stone composition. *Urology, 81*(4), 727–730.

Lin, X., Zhao, J., Zhang, W., He, L., Wang, L., Li, H., et al. (2021). Towards screening the neurotoxicity of chemicals through feces after exposure to methylmercury or inorganic mercury in rats: A combined study using gut microbiome, metabolomics and metallomics. *Journal of Hazardous Materials, 409*, 124923. https://doi.org/10.1016/j.jhazmat.2020.124923

Liu, C.-C., Hsieh, T.-J., Wu, C.-F., Lee, C.-H., Tsai, Y.-C., Huang, T.-Y., et al. (2020). Interrelationship of environmental melamine exposure, biomarkers of oxidative stress and early kidney injury. *Journal of Hazardous Materials, 396*, 122726. https://doi.org/10.1016/j.jhazmat.2020.122726

Lotti, P., Milani, S., Merlini, M., Joseph, B., Alabarse, F., & Lausi, A. (2020). Single-crystal diffraction at the high-pressure Indo-Italian beamline Xpress at Elettra, Trieste Lotti Paolo. *Journal of Synchrotron Radiation, 27*, 222–229. https://doi.org/10.1107/S1600577519015170

Madore, F., Stampfer, M. J., Rimm, E. B., & Curhan, G. C. (1998). Nephrolithiasis and risk of hypertension. *American Journal of Hypertension, 11*(1), 46–53. https://doi.org/10.1016/s0895-7061(97)00371-3

Mandel, S., & Tas, A. C. (2010). Brushite (CaHPO4·2H2O) to octacalcium phosphate (Ca8(HPO4)2(PO4)4·5H2O) transformation in DMEM solutions at 36.5 °C. *Materials Science and Engineering C, 30*, 245–254. https://doi.org/10.1016/j.msec.2009.10.009

mindat.org. (n.d.-b). https://www.mindat.org/min-793.html

mindat.org. (n.d.-a). https://www.mindat.org/min-4276.html

Moran, M. E. (2014). *Urolithiasis: A Comprehensive History*. (Springer Nature, Ed.) (1st ed.). Springer.

Moser, R., Zaccarini, F., Alber, T., & Kerbl, R. (2020). First finding of tiemannite, HgSe, in human bladder stones: An electron microprobe study. *Micron, 138*, 102928.

Mukherjee, A. K. (2014). Human kidney stone analysis using X-ray powder diffraction. *Journal of the Indian Institute of Science, 94*(1), 35–44.

Mulongo-Masamba, R., El Kassri, T., Khachani, M., Arsalane, S., Halim, M., & El Hamidi, A. (2016). Synthesis and thermal dehydroxylation kinetic of anhydrous calcium phosphate monetite CaHPO4. *Journal of Thermal Analysis and Calorimetry, 124*, 171–180. https://doi.org/10.1007/s10973-015-5130-y

Muschietti, L., Orto, V., & Garrido, G. (2016). Infrared Spectroscopic Analysis of Urinary Calculi: A Retrospective Study in Argentinean Patients. *Asian Journal of Medicine and Health, 1*(3), 1–9. https://doi.org/10.9734/ajmah/2016/29354

Nair, C. G. R., & Ninan, K. N. (1978). Thermal decomposition studies: Part X. Thermal decomposition kinetics of calcium oxalate monohydrate—correlations with heating rate and samples mass. *Thermochimica Acta, 23*(1), 161–169.

Öhman, S., Larsson, L., & Tiselius, H.-G. (1992). Clinical significance of phosphate in calcium oxalate renal stones. *Annals of Clinical Biochemistry, 29*(1), 59–63.

Pal'chik, N. A., Moroz, T. N., Maksimova, N. V., & Dar'in, A. V. (2006). Mineral and microelement compositions of urinary stones. *Russian Journal of Inorganic Chemistry, 51*(7), 1098–1105. https://doi.org/10.1134/S0036023606070138

Perlmutter, S., Hsu, C. T., Villa, P. A., & Katz, D. S. (2002). Sonography of a human jackstone calculus. *Journal of Ultrasound in Medicine, 21*, 1047–1051. https://doi.org/10.7863/jum.2002.21.9.1047

Prien, E. L., & Frondel, C. (1947). Studies in urolithiasis; the composition of urinary calculi. *The Journal of Urology, 57*(6), 949–991. https://doi.org/10.1016/s0022-5347(17)69732-5

Primiano, A., Persichilli, S., Gambaro, G., Ferraro, P. M., D'Addessi, A., Cocci, A., et al. (2014). FT-IR analysis of urinary stones: A helpful tool for clinician comparison with the chemical spot test. *Disease Markers*. https://doi.org/10.1155/2014/176165

Ringertz, H. (1965). Optical and crystallographic data of uric acid and its dihydrate. *Acta Crystallographica, 19*, 286. https://doi.org/10.1107/s0365110x65003298

Rivell, C. G., & Coren, J. S. (2012). Onesies, Twosies, not a game of Jackstones. *Osteopathic Family Physician, 4*, 88–90. https://doi.org/10.1016/j.osfp.2011.10.002

Schnitzler, E., Kobelnik, M., Sotelo, G. F. C., Bannach, G., & Ionashiro, M. (2004). Thermoanalytical study of purine derivatives compounds. *Ecletica Quimica, 29*(1), 71–78. https://doi.org/10.1590/S0100-46702004000100009

Schubert, G. (2006). Stone analysis. *Urological Research, 34*, 146–150. https://doi.org/10.1007/s00240-005-0028-y

Sekkoum, K., Cheriti, A., Taleb, S., & Belboukhari, N. (2016). FTIR spectroscopic study of human urinary stones from El Bayadh district (Algeria). *Arabian Journal of Chemistry, 9*, 330–334. https://doi.org/10.1016/j.arabjc.2011.10.010

Selvaraju, R., Raja, A., & Thiruppathi, G. (2015). FT-IR spectroscopic, thermal analysis of human urinary stones and their characterization. *Spectrochimica Acta - Part A: Molecular and Biomolecular Spectroscopy, 137*, 1397–1402. https://doi.org/10.1016/j.saa.2014.09.046

Shiekh, F. A., Khullar, M., & Singh, S. K. (2006). Lithogenesis: Induction of renal calcifications by nanobacteria. *Urological Research, 34*(1), 53–57.

Siener, R., Glatz, S., Nicolay, C., & Hesse, A. (2004). The role of overweight and obesity in calcium oxalate stone formation. *Obesity Research, 12*(1), 106–113. https://doi.org/10.1038/oby.2004.14

Singh, K. J., Tiwari, A., & Goyal, A. (2011). Jackstone: A rare entity of vesical calculus. *Indian Journal of Urology*. https://doi.org/10.4103/0970-1591.91449

Singh, V. K., & Rai, P. K. (2014). Kidney stone analysis techniques and the role of major and trace elements on their pathogenesis: A review. *Biophysical Reviews, 6*, 291–310. https://doi.org/10.1007/s12551-014-0144-4

Sivaguru, M., Saw, J. J., Williams, J. C., Lieske, J. C., Krambeck, A. E., Romero, M. F., et al. (2018). Geobiology reveals how human kidney stones dissolve in vivo. *Scientific Reports, 8*, 13731. https://doi.org/10.1038/s41598-018-31890-9

Słojewski, M. (2011). Major and trace elements in lithogenesis. *Central European Journal of Urology, 64*(2), 58.

Subasinghe, D., Goonewardena, S., & Kathiragamathamby, V. (2017). Jack stone in the bladder: Case report of a rare entity. *BMC Urology, 17*, 40. https://doi.org/10.1186/s12894-017-0230-6

Suryawanshi, V. B., & Chaudhari, R. T. (2014). Growth and characterization of agar gel grown brushite crystals. *Indian Journal of Materials Science*. https://doi.org/10.1155/2014/189839

Sweeney, A. P., & Dyer, R. B. (2015). The "jackstone" appearance. *Abdominal Imaging, 40*, 2906–2907. https://doi.org/10.1007/s00261-015-0440-x

Türk, C, Donaldson, J. F., Neisius, A., Petrik, A., Skolarikos, A., & Thomas, K. (2019). *EAU Guideline: Bladder Stones*. https://uroweb.org/guideline/bladder-stones/

Türk, C., Petřík, A., Sarica, K., Seitz, C., Skolarikos, A., Straub, M., & Knoll, T. (2016). EAU guidelines on interventional treatment for urolithiasis. *European Urology*. https://doi.org/10.1016/j.eururo.2015.07.041

Turney, B. W., Appleby, P. N., Reynard, J. M., Noble, J. G., Key, T. J., & Allen, N. E. (2014). Diet and risk of kidney stones in the Oxford cohort of the European Prospective Investigation into Cancer and Nutrition (EPIC). *European Journal of Epidemiology, 29*(5), 363–369.

Wang, C. J., Hsu, C. S., Chen, H. W., Tsai, P. C., & Chang, C. H. (2016). Long-term effects of lemonade therapy on hypocitraturic nephrolithiasis and stone recurrence: A mini review. *International Journal of Nephrology and Kidney Failure, 2*(1), 1–4.

Wang, L., Chen, M., He, P., Yu, H., Block, K. A., & Xie, Z. (2019). Composition and spatial distribution of elements and isotopes of a giant human bladder stone and environmental implications. *Science of the Total Environment, 650*, 835–846.

Wilson, E. V., Bushiri, M. J., & Vaidyan, V. K. (2010). Characterization and FTIR spectral studies of human urinary stones from Southern India. *Spectrochimica Acta - Part A: Molecular and Biomolecular Spectroscopy, 77*, 442–445. https://doi.org/10.1016/j.saa.2010.06.014

Zhao, W., Sharma, N., Jones, F., Raiteri, P., Gale, J. D., & Demichelis, R. (2016). Anhydrous calcium oxalate polymorphism: A combined computational and synchrotron X-ray diffraction study. *Crystal Growth & Design, 16*(10), 5954–5965.